



# A Global Optimizer for Nanoclusters

Maya Khatun, Rajat Shubhro Majumdar and Anakuthil Anoop\*

Department of Chemistry, Indian Institute of Technology Kharagpur, Kharagpur, India

We have developed an algorithm to automatically build the global minimum and other low-energy minima of nanoclusters. This method is implemented in PyAR (<https://github.com/anooplabs/pyar>) program. The global optimization in PyAR involves two parts, generation of several trial geometries and gradient-based local optimization of the trial geometries. While generating the trial geometries, a Tabu list is used for storing the information of the already used trial geometries to avoid using the similar trial geometries. In this recursive algorithm, an  $n$ -sized cluster is built from the geometries of  $n - 1$  clusters. The overall procedure automatically generates many unique minimum energy geometries of clusters with size from 2 up to  $n$  using this evolutionary growth strategy. We have used our strategy on some of the well-studied clusters such as Pd, Pt, Au, and Al homometallic clusters, Ru-Pt and Au-Pt binary clusters, and Ag-Au-Pt ternary cluster. We have analyzed some of the popular parameters to characterize the clusters, such as relative energy, singlet-triplet energy difference, binding energy, second-order energy difference, and mixing energy, and compared with the reported properties.

## OPEN ACCESS

### Edited by:

Emilio Martinez-Nunez,  
University of Santiago de Compostela,  
Spain

### Reviewed by:

Scott Hopkins,  
University of Waterloo, Canada  
Jadson Claudio Belchior,  
Federal University of Minas Gerais,  
Brazil

### \*Correspondence:

Anakuthil Anoop  
[anoop@chem.iitkgp.ac.in](mailto:anoop@chem.iitkgp.ac.in)

### Specialty section:

This article was submitted to  
Theoretical and Computational  
Chemistry,  
a section of the journal  
Frontiers in Chemistry

Received: 31 May 2019

Accepted: 09 September 2019

Published: 27 September 2019

### Citation:

Khatun M, Majumdar RS and  
Anoop A (2019) A Global Optimizer for  
Nanoclusters. *Front. Chem.* 7:644.  
doi: 10.3389/fchem.2019.00644

**Keywords:** global optimization, PyAR, nanocluster, binary cluster, ternary cluster, nanoalloys, cluster builder

## 1. INTRODUCTION

A major focus in modern nanoscience is to understand the properties of materials on the atomic scale (Eberhardt, 2002). Subnanometer scale metal clusters are of great interest due to their structural and electronic properties (Baletto and Ferrando, 2005), which makes them useful for applications in various field like nanotechnology, electronics, medical device and catalysis (Saha et al., 2012). The atomic clusters may comprise of atoms of the same element such as fullerenes or atoms of different elements as in nanoalloys (Johnston, 2002). A molecular-level understanding of small nanoclusters would provide insights into the largely empirical field of nanoscience.

Theoretical study of nanoclusters can help us to understand the smooth transition from atoms to bulk materials, especially the size-dependent evolution of the properties (Jortner, 1992; Edwards et al., 1998). The primary input for the theoretical study is their geometry. While determining the geometry of nanoclusters by experiments is extremely difficult, the atomic structure of clusters can be predicted theoretically by geometry optimization tools that are specifically designed for global optimization (Zhao et al., 2017).

Global optimization of functions is an essential part of various research fields and have many real-life applications (Floudas and Gounaris, 2008; Barbati et al., 2012; Khare and Rangnekar, 2013). The global optimization (GO) is the process of finding the best solution, “global maximum” or “global minimum” (GM), based on one or more criteria for a mathematically formulated function (Jäger et al., 2018). The global optimization in our context refers to finding the most stable geometry for a particular cluster, that is the lowest energy atomic arrangements on the potential energy surface (PES). The global minima of atomic clusters (Davis et al., 2015; Shayeghi et al., 2015a) are essential as these are often the most likely structure to be formed in the experiment. Thus, finding

the global minimum and other low-lying minima on the PES is helpful to interpret the experimental results (Shayeghi et al., 2014, 2015b; Götz et al., 2016).

The efficiency of geometry optimization (GO) algorithm is crucial for the success in the attempts to understand the cluster science. Some of the popular GO algorithms are Genetic Algorithms (GA) (Johnston, 2003), Basin Hopping (BH) (Wales and Scheraga, 1999), Particle Swarm Optimization (PSO) (Lv et al., 2012; Shi et al., 2019), Artificial Bee Colony (ABC) (Zhang and Dolg, 2015), Simulated Annealing (Kirkpatrick et al., 1983), Threshold Algorithms (Schön et al., 1996) etc. These general GO algorithms are employed in the studies of metal clusters with varying degrees of success. As for any applications of GO, there is no universal method that works for all the molecular systems in chemistry and is an open area of research.

A major challenge in any GO method is the computational complexity, the exponential increase in the search space with system size (Doye and Wales, 1998). A GO algorithm must combine a locally confined search with the wide exploration of the regions without revisiting the same regions (Heiles and Johnston, 2013) in the PES in a computationally effective way. The fine balance of local search and global exploration is required. The re-examination of a minimum only gives redundant information wasting computational resources. On the other hand, confining the search only to a small neighboring area does not allow the algorithm to find the GM in other funnels on the PES. Metadynamics algorithms overcome the revisiting problem by adding time-dependent repulsive bias potential function of collective variables to discourage revisiting the already visited areas. Tabu-search based algorithms (Glover, 1986, 1989, 1990) store the information of previously visited areas to avoid the searching of the already explored region.

In this article, we explain our strategy to find the global minima geometries of atomic clusters—unary, binary and ternary nanoclusters. We have combined two strategies to improve the efficiency: the Tabu-search algorithm to reduce the time spent on the already found minima and a novel recursive approach to reduce the search space by making use of the solutions from the smaller problem. That is, we build the solutions of  $n$  sized cluster based on the solutions of  $n - 1$  sized cluster. This way, the unique geometries of cluster size  $n$  can be built bottom-up starting from the single atom. This method is particularly useful for studying the evolution of structure and properties with the growth of cluster size. We have discussed the implementation and the validation by applying on the known metallic clusters. We have compared the geometries and a few representative properties of the clusters generated by our algorithm with the reported geometries and corresponding properties.

## 2. THEORETICAL APPROACH

### 2.1. Cluster Building and Optimization

Our method for the global optimization of the geometries of atomic clusters is an adaptation of our approach for the automated exploration of reaction and aggregation implemented in PyAR (Nandi et al., 2017; Anoop, 2019) program. In this section, we will explain the philosophy and implementation of

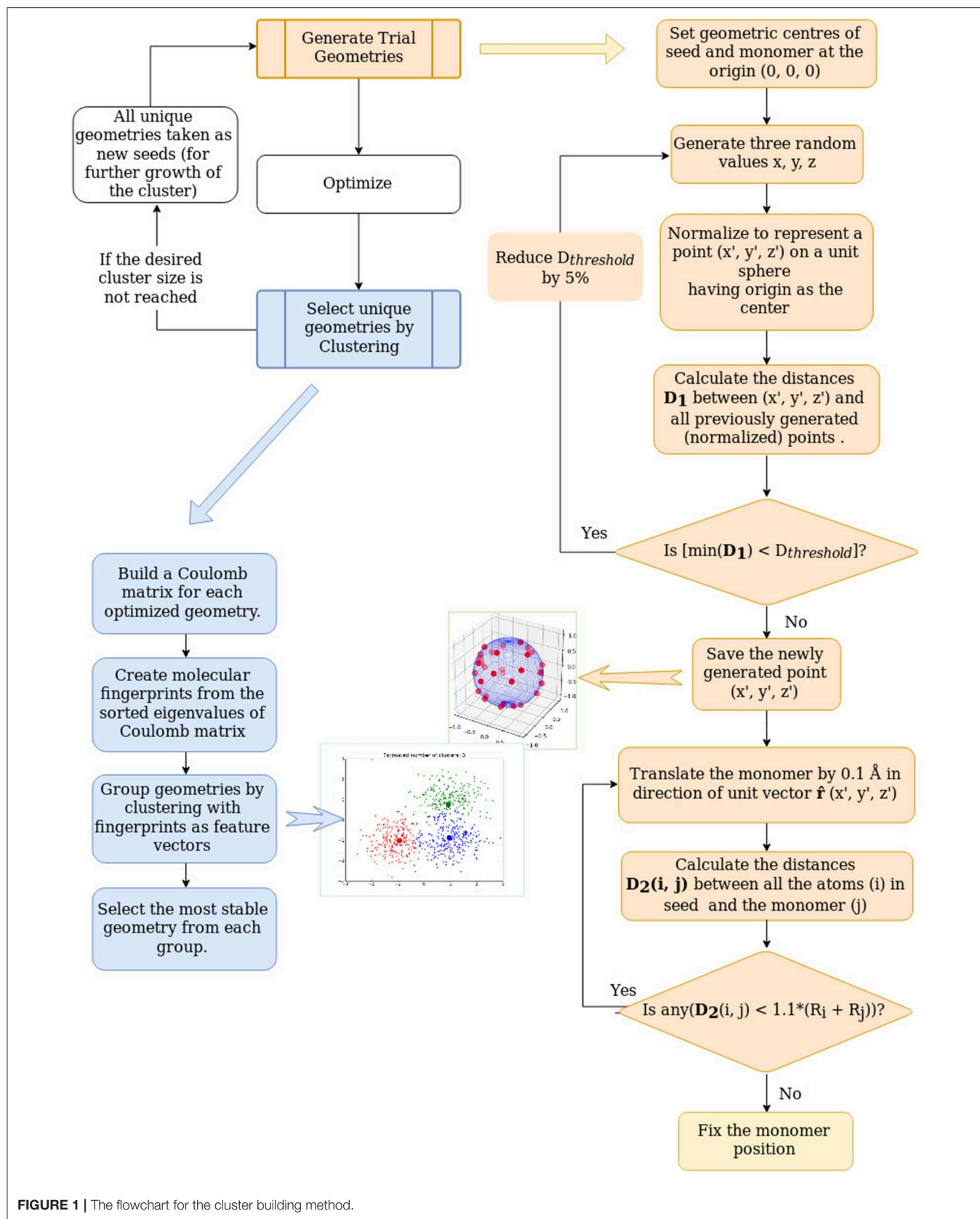
the aggregator modules used for the building of nanoclusters (Figure 1). The global optimization for nanoclusters in PyAR involves two parts, generation of several trial geometries and gradient-based local optimization of these trial geometries. In our algorithm, the search for solutions of  $n$ -sized cluster make use of the solutions from the search on the  $n - 1$  sized clusters. At each cycle, the problem is reduced to find the best relative orientations between two species. This approach is analogous to finding the solution of the traveling salesman problem with  $N$  cities by adding one more city to the solution of the problem with  $N-1$  cities. The overall procedure automatically generates several unique minimum energy geometries of clusters with size up to  $n$  using our evolutionary growth strategy.

This process can be imagined as growing the cluster by adding atoms one by one. The method is similar to the cluster-fusion algorithm of Solov'yov et al. (2004). When the second atom is added to the first one, there is only one possible geometry and there is only one variable—the distance between the atoms. The trial geometry for the dimer is generated as follows. The first atom (called as seed) is placed at the origin of the Cartesian coordinate system. For placing the second atom (named monomer), the value for the  $x$ -coordinate is generated as a random number between 0 and 1. Then, the value of  $x$  is increased in small steps of 0.1 Å until  $x$  is larger than the sum of covalent radii of both atoms ( $x > (R_a + R_b)$ ). This way, the second atom is placed in the  $X$ -axis at a distance of no close-contact between the atoms.

The third atom could be placed anywhere in the  $xy$ -plane at a distance from the existing atoms of the dimer avoiding close-contacts. Here, the dimer is the seed, and the atom is the monomer. The  $xy$ -plane (the search space) is divided into four quadrants. The new atoms are placed in each quadrant sequentially. The quadrant is chosen by generating random numbers for  $x$  and  $y$  coordinates within a suitable range to fit a particular quadrant. The new coordinates created by these random numbers are normalized so that the point is at a unit distance from the origin. As described above, the third atom initially placed at this position is translated away from the origin to avoid any close contacts.

The search space for the addition of the fourth atom and further on is three-dimensional. The 3D space around the trimer (and larger  $n$ 'mers) is divided into eight octants. The new atoms are placed in random positions at unit distance from the origin in each of these octants sequentially. The reason for dividing the space into octants is to distribute the new trial geometries evenly so that even with a few trial geometries, there is a chance of exploring different region of space and getting dissimilar geometries. This way,  $N$  trial geometries are generated.  $N$  is a user-provided parameter. All the trial geometries will be optimized using local, gradient-based optimizers. The optimizations are done by the interfaced software as described later in this section.

Some of the optimized geometries obtained by the gradient-based optimization of these trial geometries may belong to the same minima in the PES, with small differences in geometrical parameters depending on the convergence criteria. Comparison of geometries based on Cartesian coordinates such as RMSD of the atomic positions may fail because the optimization may



reorient the molecule, and the Cartesian coordinates are not rotationally invariant. Besides, the same geometry with different ordering of atoms will also be shown as different geometries by such comparisons. Therefore, we have implemented various molecular representations to find the similarity.

One of such representations that we have used in this work is the molecular fingerprints, computed as follows. An  $n$ -by- $n$  matrix, known as Coulomb matrix (Rupp et al., 2012; Sadeghi et al., 2013), is made in which the off-diagonal elements are the pairwise Coulomb repulsions  $\frac{Z_i Z_j}{R_{ij}}$ , and the diagonal elements are  $Z_i^2/2$ . The  $Z_i$  and  $Z_j$  are the core charge of atom  $i$  and  $j$ . The Coulomb matrix is diagonalized. The sorted eigenvalues are considered as the molecular fingerprints. The fingerprint is used as the feature vector for clustering algorithm (see below) and the euclidean distance between the fingerprints is used as the measure of similarity.

Using the molecular fingerprint representation, these optimized geometries are analyzed and clustered into groups (up to 8 clusters) of similar geometries using clustering algorithms (Nandi et al., 2018) in Scikit-learn (Pedregosa et al., 2011) python library. The most stable geometry from each of these clusters are selected as the minima for this  $n$ 'mer and the most stable among the minima is the global minimum geometry for this  $n$ 'mer. All of these minima are considered for further growth by adding a new atom. This way the degree of freedom of  $n$ 'mer ( $3N - 6$ ) is reduced to 3.

Besides the reduction in complexity, the other significant improvement to increase the efficiency is to avoid revisiting the already visited regions. In our context, we store all the randomly created points and compare the new point with the stored points. For a reasonable comparison, all the positions are generated at a unit distance from the origin, i. e. positions lie on the surface of the sphere of a unit radius (1 Å). If the new position is within the threshold distance from any of the stored positions, the new position is rejected. This threshold distance is initially set as 0.3 Å and is increased by 5 % in each cycle. As this idea is adapted from Tabu-search algorithm (Glover, 1986, 1989, 1990), the list of stored positions is referred as the Tabu list. This method of filtering the position makes sure that the trial geometries are sufficiently dissimilar.

The  $N$  trial geometries created by the method explained above will be optimized with the electronic structure programs that are interfaced with PyAR. Currently we have interfaced with Gaussian 09/16 (Frisch et al., 2016), MOPAC (Stewart, 2016), PSI4 (Turney et al., 2012), ORCA (Neese, 2018), Turbomole (Furche et al., 2014), XTb (Grimme et al., 2017). The user can choose the program and the methods (functional-basis set, semiempirical method). There are few rounds of optimizations. The full set of trial geometries will be initially optimized by loose convergence setting. After filtering similar geometries based on the similarity based on molecular fingerprints, a smaller set of selected geometries will be optimized with standard convergence criteria. In principle, we can also make the automatic procedure to use initial screening with fast and less accurate methods followed by calculations with slow and more accurate methods on a smaller number of geometries.

The methodology described above is for the homometallic clusters. We have extended the procedure to create the binary, ternary and other heteroatomic clusters that are even more interesting and challenging. For making binary clusters, we use both the input atoms as the seed and the monomer instead of one being the seed and the other as the monomer. The procedure, implemented as `binary_aggregator`, generates all combinations of binary clusters of size ranging from  $A_1B_1$  to  $A_mB_n$ . The algorithm first treats "A" as the seed and "B" as the monomer and repeats the cycle until the number of "B" atoms reaches  $n$ . Hence, the row of the matrix is built ranging from  $A_1B_1$  till  $A_1B_n$ . When B is considered as seed and A as the monomer, another row is built ranging from  $A_1B_1$  till  $A_mB_1$ . Similarly, by using  $A_xB_y$ ,  $x < m$  and  $y < n$ , other rows of the matrix can be generated.

We added another layer over the `binary_aggregator` to build the ternary clusters by including a third element. The `ternary_aggregator` operates analogously by adding the element C sequentially to each combination of binary clusters made by `binary_aggregator`. The new monomer is added until it reaches its desired size of the third element. Thus, for each of the binary cluster ( $A_iB_j$ ;  $i = 1-m$ ,  $j = 1-n$ ), the 3rd element is added as a monomer to generate ternary clusters ranging from  $(A_mB_nC_1)$  to  $(A_mB_nC_l)$  where  $l$  is the maximum number of element C.

Current procedures for binary and ternary clusters are expensive because we used exhaustive enumeration. Exhaustive exploration is required until we find some guiding principles for understanding the mixing behaviors of these alloys.

## 2.2. Properties of Clusters

The relative stabilities of the clusters built using the above described methods can be calculated using the following popular parameters.

### 2.2.1. Homometallic Clusters

#### 2.2.1.1. Relative energy (RE/eV):

The energy of a cluster compared with the most stable isomer (GM). The higher RE means a lower stability.

#### 2.2.1.2. Singlet triplet energy difference ( $\Delta E_{ST}/eV$ ):

The energy difference between the singlet and triplet state is  $\Delta E_{ST} = E_{triplet} - E_{singlet}$ . The cluster with a positive  $\Delta E_{ST}$  has a singlet ground state, and the cluster with a negative  $\Delta E_{ST}$  has a triplet ground state.

#### 2.2.1.3. Binding energy per atom (BE/eV):

The binding energy per atom (BE or BEPA) is calculated by Equation (1):

$$BE = \frac{1}{N}[E_n - nE_1] \quad (1)$$

where,  $E_n$  is energy of  $n$  atomic cluster;  $n$  is the cluster size or aggregation number;  $E_1$  is the energy of an atom.

### 2.2.1.4. Second-order energy difference ( $\delta^2 E(n)$ , SOD/eV):

The SOD indicates the higher stability of a cluster of  $N$  atoms relative to its heavier and lighter neighbors. Therefore,  $\delta^2 E(n)$  is more relevant in interpreting experimental mass spectral intensities than the BE (Rogan et al., 2005). Large maxima of  $\delta^2 E(n)$  shows the higher probability of finding these clusters.

$$\delta^2 E(n) = E_{n+1} + E_{n-1} - 2E_n \quad (2)$$

where,  $E_{n+1}$  is the total energy of  $n + 1$  atomic cluster;  $E_{n-1}$  is the total energy of  $n - 1$  atomic cluster;  $E_n$  is the total energy of  $n$  atomic cluster; and  $n$  is the cluster size.

## 2.2.2. Energy Parameters for Binary and Ternary Nanoalloys

### 2.2.2.1. Binding energy per atom (BE/eV):

The BE for binary and ternary clusters (Song et al., 2005; Demiroglu et al., 2017) is given by Equations (3) and (4):

$$E_b = \frac{1}{N} [E_{tot}(A_m B_n) - mE_{tot}(A_1) - nE_{tot}(B_1)] \quad (3)$$

$$E_b = \frac{1}{N} [E_{tot}(A_m B_n C_l) - mE_{tot}(A_1) - nE_{tot}(B_1) - lE_{tot}(C_1)] \quad (4)$$

where,  $m$ ,  $n$ , and  $l$  are the numbers of A, B, and C atoms;  $E_{tot}(A_1)$ ,  $E_{tot}(B_1)$ , and  $E_{tot}(C_1)$  are the electronic energies of a single A, B or C atom and  $N$  is the total number of atoms ( $N = m + n + l$ ) in the particular cluster.

### 2.2.2.2. Mixing energy (ME/eV):

The mixing energy (Song et al., 2005; Pacheco-Contreras et al., 2018) is an indicator of the stability of the binary cluster with respect to its unary counterpart, given by Equation (5):

$$\delta = E_{tot}(A_m B_n) - m \frac{E_{tot}(A_{m+n})}{m+n} - n \frac{E_{tot}(B_{m+n})}{m+n} \quad (5)$$

where,  $E_{tot}(A_m B_n)$  is the total energy of the alloy,  $E_{tot}(A_{m+n})$  and  $E_{tot}(B_{m+n})$  are the total energies of the pure metal clusters, A and B of the same size ( $m + n$ ). A negative value of  $\delta$  means a decrease of energy upon mixing and therefore, a favorable mixing.

## 3. COMPUTATIONAL DETAILS

We used the PyAR program to build the clusters, primarily with the Tight-Binding semi-empirical method, GFN-xTB, with the XTB program (Grimme et al., 2017). This combination is denoted as PyAR|XTB. In a few cases, the selected geometries from PyAR|XTB were reoptimized using PBE0 (Adamo and Barone, 1999) functional and def2-TZVP basis set with the ORCA4.0.1.2 (Neese, 2018) program. These minima from PBE0/def2-TZVP was characterized as true minima with no imaginary frequency. This combined method is denoted as PyAR|XTB||PBE0. We have used another combination where the clusters are built using the ORCA program as the interface using the PBE functional or the BP86 (Perdew, 1986; Becke, 1988) functional and the def2-SVP basis set (Weigend and Ahlrichs, 2005), denoted as

PyAR|ORCA. We have added Grimme's dispersion corrections (D3-BJ) (Grimme et al., 2011) in all DFT calculations. We have used effective core potential (ECP) (Pettersson et al., 1983) in the DFT calculations to add the relativistic effect for all the transition metals.

## 4. RESULTS AND DISCUSSION

We have built various metal clusters—homometallic nanoclusters, bimetallic and trimetallic nanoalloys. In this work, our focus was to validate our approach for its ability to generate the global minimum (GM) and other unique local minima and reproduce the qualitative trends in various properties. Therefore, we have chosen the clusters and alloys that are studied extensively—Pd, Au, Pt, and Al homometallic clusters and Ru-Pt, Au-Pt, Ag-Au-Pt nanoalloys. We have compared the GM geometries and few other low-lying local minima with the corresponding reported geometries. We calculated few properties such as relative energy, binding energy, singlet-triplet energy difference, second-order energy difference, and mixing energy of the clusters and alloys made by our program and compared with the values and trends reported in the literature. Due to the difference in electronic structure theories in different studies, differences are expected in absolute numbers, but overall trends were similar.

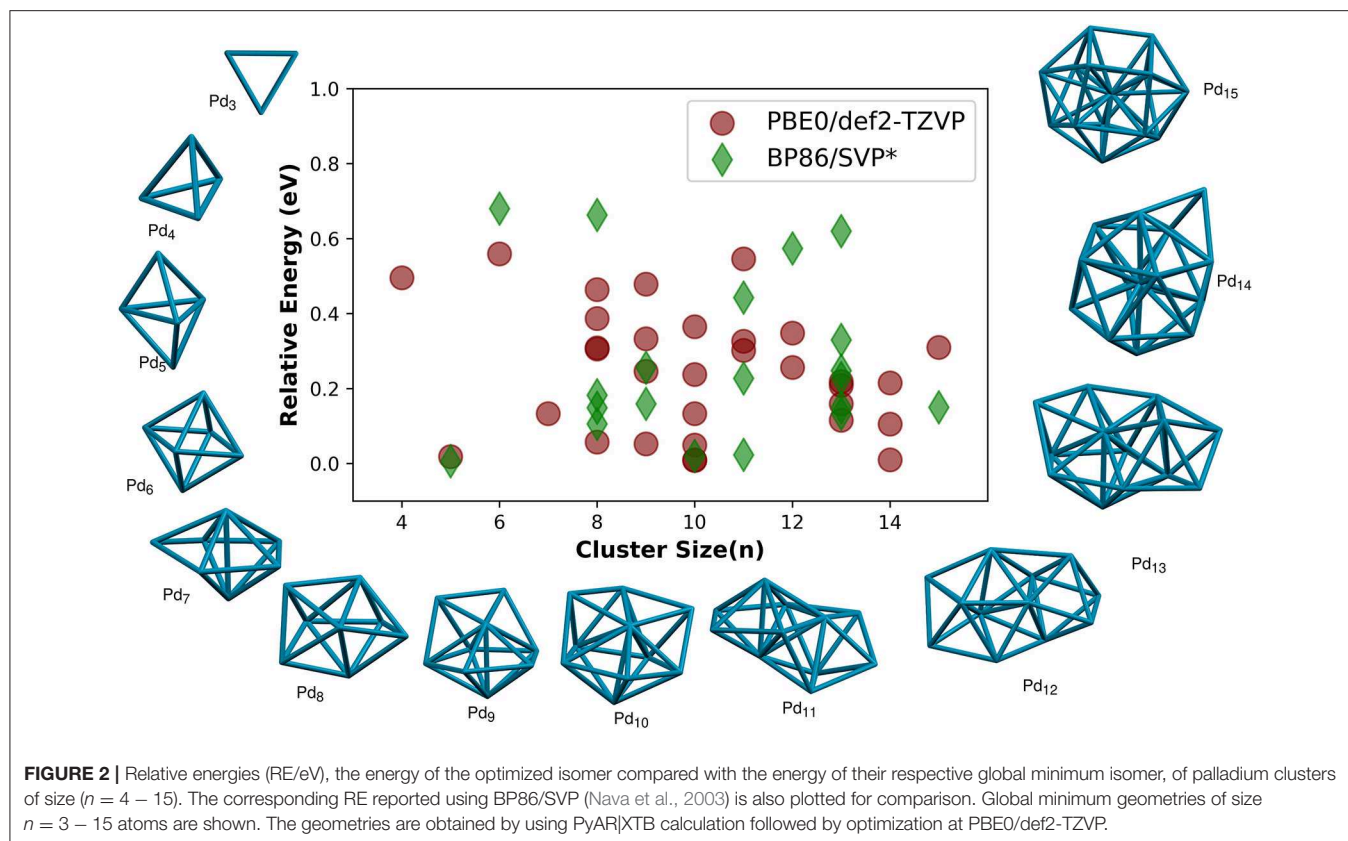
### 4.1. Homometallic Nanoclusters

#### 4.1.1. Palladium

The first example for this study of nanoclusters is the palladium nanoclusters. We have located the unique geometries of Pd<sub>n</sub> ( $n=2-15$ ) clusters using our algorithm implemented in PyAR program. We used two different methods for the global optimization, PyAR|XTB and PyAR|ORCA(PBE). We have also used a two-layer approach in which the search for geometries is done by one method and the selected geometries are optimized again at a different method. For example in the method named as PyAR|XTB||PBE0, the search was done with PyAR|XTB and the geometries selected by this method were further optimized with PBE0. We have employed two more DFT functionals in this study, PyAR|XTB||B3LYP and PyAR|XTB||M06. We have further compared the geometries of Pd<sub>n</sub> clusters in singlet and triplet electronic states. The global minimum geometries of singlet Pd<sub>n</sub> clusters are shown in **Figure 2**.

Only one minimum was found for triatomic palladium clusters, Pd<sub>3</sub>, which has a triangular geometry. The shape of Pd<sub>3</sub> is slightly distorted from the equilateral triangle with the base angle of 59.9°; such non-equilateral geometry was also reported by Nava et al. (2003). The average bond length and bond dissociation energy are 2.54 Å and 2.57 eV at PBE0/def2-TZVP compared to the values from CAS/MRSDCI level calculation (Balasubramanian, 1989) which are 2.67 Å and 3.28 eV.

As the cluster size grew, the program has selected more than one unique structures for clusters with  $n = 4-15$ . The relative energies (RE, the energy compared to the global minimum isomer) of all the non-global-minimum geometries are shown in **Figure 2**, along with the results from Nava et al. (2003)



for comparison. All the larger  $Pd_n$  clusters,  $n > 3$ , have three-dimensional global minima. Some of these GM geometries are discussed below.

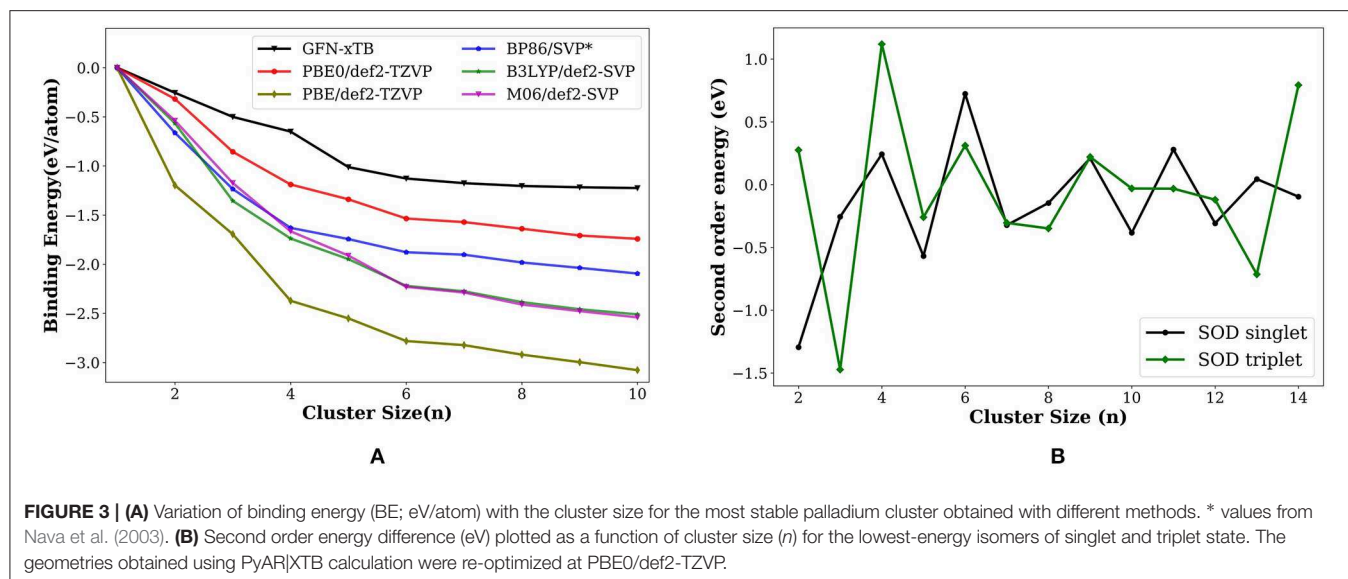
The most stable structure for  $Pd_4$  cluster is tetrahedral. Bond dissociation energy is 4.77 eV at PBE0/def2-TZVP level compared to 5.07 eV at the MRSDCI level calculations (Dai and Balasubramanian, 1995). The bond length is 2.62 Å at PBE0/def2-TZVP, 2.68 Å at MRSDCI (Dai and Balasubramanian, 1995) and 2.61 Å using other DFT calculations (Xiao et al., 1999). We found another minimum, a bicyclic, non-planar, *butterfly*-like geometry, not reported before, which is 0.50 eV higher in energy than the tetrahedral GM structure. Global minimum geometry of  $Pd_5$  is trigonal bipyramid. The average bond length in this geometry is 2.74 Å, and the binding energy of the *TBP* structure we calculated at PBE0/def2-TZVP is 1.34 eV, similar to the reported values from the DFT calculation (Wen et al., 2018) using GGA functional (BP/DNP), 2.704 Å and 1.73 eV, respectively. The  $Pd_6$  cluster has an octahedral global minimum. Thus, the most symmetric platonic geometries—trigonal, tetrahedral, trigonal bipyramidal, and octahedral—are the global minima for  $Pd_3$ - $Pd_6$ .

The most stable geometry of  $Pd_7$  from the PyAR|XTB calculations is pentagonal bipyramidal (PBP), but is a non-platonic geometry, octahedral core with one cap when PBE and PBE0 methods were used. The PBP was not a minimum, and the trigonal bipyramid with two caps is the next higher energy isomer that has a RE of 0.13 eV compared to GM in PBE0. In the triplet

state, the PBP is the most stable structure at BP86 (Nava et al., 2003) and BLYP (Rogan et al., 2005) levels. According to Nava et al. (2003), the mono-capped octahedral and bicapped-TBP  $Pd_7$  are only 0.03 eV and 0.05 eV higher in energy, respectively, compared to the most stable PBP.

The symmetric dodecahedral geometry was found to be the lowest energy cluster for  $Pd_8$ . From  $Pd_8$  to  $Pd_{13}$ , pentagonal bipyramidal (PBP) based structures dominate the global minima. For  $Pd_{13}$ , the most symmetrical icosahedral structure is not the GM in our calculation (R.E. = 0.21 eV), in agreement with the calculations by Nava et al. (2003) and Reveles et al. (2012) in which the symmetric geometry is higher in energy compared to the most stable geometry by 0.13 eV (BP86/SVP) and 0.16 eV (PBE/DZVP), respectively. The  $Pd_{14}$  has an icosahedral core with one cap.

We have calculated the selected geometries in the triplet state as the report (Nava et al., 2003) suggested that many of the Pd clusters have triplet ground states. The  $\Delta E_{ST}$  is shown in **Figure S1**. In PBE0, all  $Pd_n$  clusters have negative  $\Delta E_{ST}$ , i. e. have triplet ground state, except for Pd atom. The ground state of the Pd atom has a closed-shell electronic configuration. The dimer is well established as a triplet ground state in the literature (Lin et al., 1969; Zacarias et al., 1999; Nava et al., 2003), which is reproduced by our DFT result as well—the singlet  $Pd_2$  has higher energy (0.45 eV) than its triplet state. The dissociation energy of dimer is 0.64 eV which is in agreement with the experimental dissociation energy  $0.73 \pm 0.26$  eV (Lin et al., 1969) as well as



various density functional calculations done by Zacarias et al. (1999). The GFN-xTB results, however, showed that all the  $\text{Pd}_n$  clusters, except  $\text{Pd}_6$ , have singlet ground state. The  $\Delta E_{ST}$  in GFN-xTB is large positive for  $n = 1, 3$ , and 5, but are slightly positive for  $n = 2, 4, 7-15$ . Thus,  $\Delta E_{ST}$  is not well represented by GFN-xTB in this  $\text{Pd}_n$  clusters.

The binding energy per atom (BE/eV) increases as the cluster grows, the trend consistently reproduced by all methods (Figure 3A), GFN-xTB, BP86 (Nava et al., 2003), PBE, PBE0, B3LYP, and M06 calculations. The most stable geometries as well as the qualitative features in the overall binding energies gives us a promising strategy for the building of large scale clusters. We can use a two-stage approach where a semiempirical calculations is used for the exploration of minima using PyAR, followed by the optimization in DFT for the selected geometries.

The second order energy difference (SOD; Figure 3B) is useful for understanding the stability of cluster with size  $n$  compared to the clusters with size  $n - 1$  and  $n + 1$ . The computed SOD for  $\text{Pd}_n$  cluster shows that  $\text{Pd}_2$ ,  $\text{Pd}_4$ ,  $\text{Pd}_6$  are more stable than its neighbors. The clusters with even number of atoms are relatively more stable than the ones with odd number of atoms. This observation is in agreement with Rogan et al. (2005) and Wen et al. (2018) which showed that  $\text{Pd}_2$ ,  $\text{Pd}_4$ , and  $\text{Pd}_6$  are relatively stable than their neighbors.

In short, the study of  $\text{Pd}_n$  clusters show that the GM structures obtained by our methodology are in good agreement with those from the reported GM structures by other studies (Nava et al., 2003; Rogan et al., 2005). We have studied three more homometallic clusters, Au, Pt and Al, and we have focused different aspects of each clusters below.

#### 4.1.2. Gold

After the study of Pd nanoclusters, we have applied our method to explore the minima of gold clusters using PyAR|XTB(GFN-xTB) and PyAR|ORCA(BP86/def2-SVP). We have generated geometries up to  $n = 10$  with PyAR|DFT and up to 20 with

PyAR|GNF-xTB. The GM structures for  $n = 4-8$  obtained from our calculations in both the methods are identical with reported structures from CCSD(T) calculations Shi et al. (2010), Baek et al. (2017).  $\text{Au}_4$  obtained as a rhombus type structure. The global minimum of gold pentamer is W-shaped, and the hexamer is a planar triangle. The GM of  $\text{Au}_7$  has an Au capped the edge of planar triangular  $\text{Au}_6$ . The  $\text{Au}_8$  has GM where an Au is capped to each edges of a square.

For  $\text{Au}_3$ , the PyAR|BP86 run found triangular and bent geometries. While, the global minima at CCSD(T) level is triangular (Baek et al., 2017), our results at BP86, PBE and PBE0 shows the bent geometry as GM. The bent structure was not a minima with PyAR|GFN-xTB and M06 functional, the optimization resulted in a triangular geometry. Thus, other than  $\text{Au}_3$ , all the other geometries for  $\text{Au}_n$ ;  $n = 4-8$  have identical geometries in GFN-xTB and DFT.

The bond length of gold dimer is calculated as 2.472 Å by GFN-xTB and 2.543 Å by BP86 which are in good agreement with the experimental value 2.490 Å. One of the important energy parameters, cohesive energy (CE) of  $\text{Au}_2$  is 1.117 eV by our BP86 calculation. This is comparable with 1.1481 eV at the CCSD(T) level (Shi et al., 2010) and 1.1524 eV from experiment (Bishea and Morse, 1991). The CE by GFN-xTB, 4.005 eV, is too high. For the gold trimer, the calculated CE is 1.172 eV, the reported results are 1.161 eV (Shi et al., 2010) and 1.255 eV (James et al., 1994).  $\text{Au}_4$  has a CE of 1.487 eV, comparable with the CCSD(T) value of 1.556 eV (Shi et al., 2010). While the results from our BP86 calculations follow the trend with the reported CCSD(T) (Shi et al., 2010) and experimental (Bishea and Morse, 1991; James et al., 1994) results, the GFN-xTB overestimates the CE.

The GM geometries shown in Figure 4 reveal that the gold clusters have flat GM up to the cluster size of ten atoms.  $\text{Al}_{11}$  has a 3D geometry. Thus, our approach is able to capture the structure evolution from 2D geometry to 3D geometry that can be attributed to the use of multiple unique seed geometries to build the clusters rather than using only the GM geometry. All the

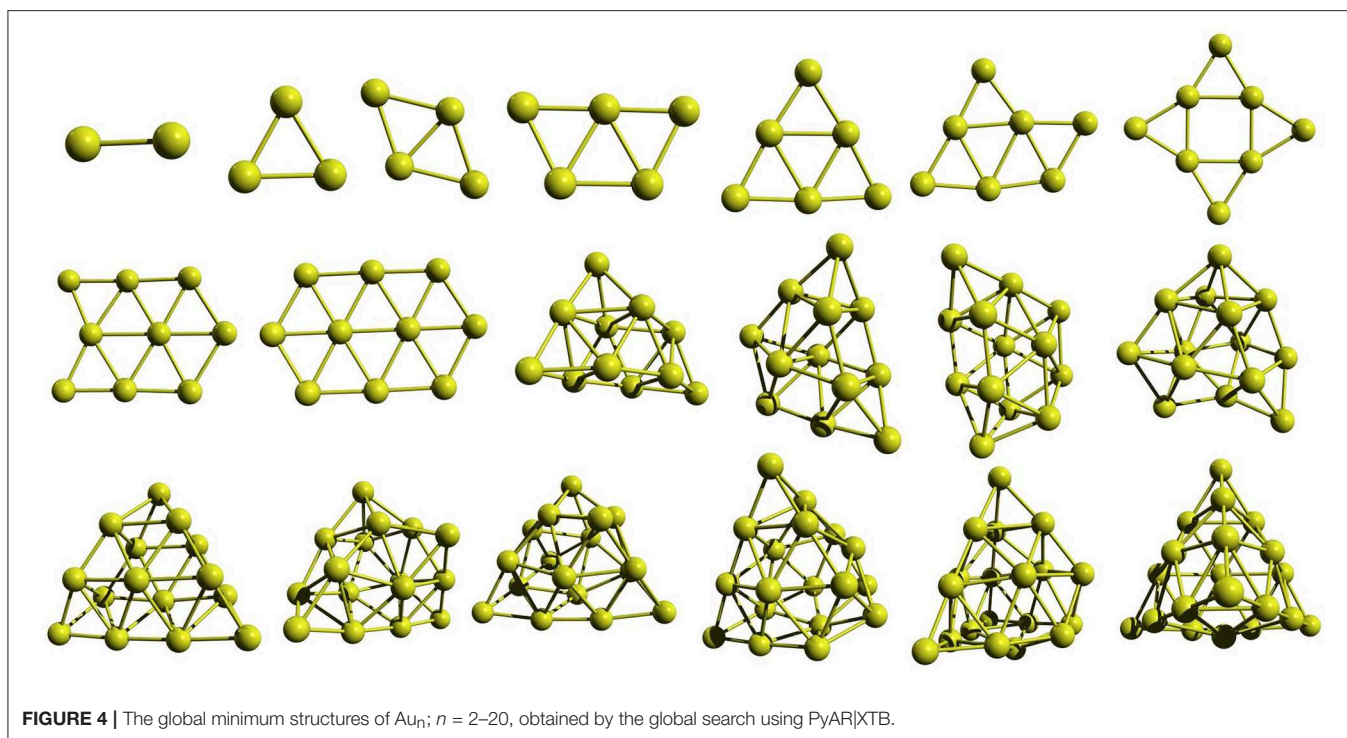


**FIGURE 4** | The global minimum structures of  $Au_n$ ;  $n = 2-20$ , obtained by the global search using PyAR|XTB.

selected geometries of  $Au_{10}$  and  $Au_{20}$  is shown in **Figure S2**. The lowest-energy isomers of  $Au_{10}$  below 0.4 eV include planar and 3D geometries—the best two are planar. As we have seen above, while the Pd clusters prefer 3D geometries throughout the size range we have studied, the gold clusters remain flat for small sizes, up to 10 in GFN-xTB and BP86 levels.

To study the effect of the number of orientations ( $N$ ) used in the run, we carried out separate runs with different values of  $N$ . As the size of the cluster increases, the  $N$  becomes more and more important. For example, the GM (shown with \*\* in **Figure S2A**) produced by one of the PyAR|XTB run with  $N = 8$  is only one of the local minima, not a GM, in the GA-DFT study (Shayeghi et al., 2015a). However, another run with more orientations along with GFN-xTB resulted in the GM from the GA-DFT and other calculations (Gotz et al., 2013; Shayeghi et al., 2015a). Similar run with DFT also produced the latter GM. The effect is more evident in the  $Au_{20}$  cluster.

The  $Au_{20}$  has a highly symmetric tetrahedral ( $T_d$ ) geometry which is one of the most often found structures in the experiment (Gruene et al., 2008) and is one of the most stable geometry in various theoretical calculations (Assadollahzadeh and Schwerdtfeger, 2009; Shayeghi et al., 2015a). The lowest-energy  $Au_{20}$  isomers in the range below 0.5 eV are shown in **Figure S2B**. Our geometries are comparable to the ones from previously studied GA-DFT, BH-DFT calculations and the experimental result (Gruene et al., 2008; Shayeghi et al., 2015a; Zhao et al., 2017).

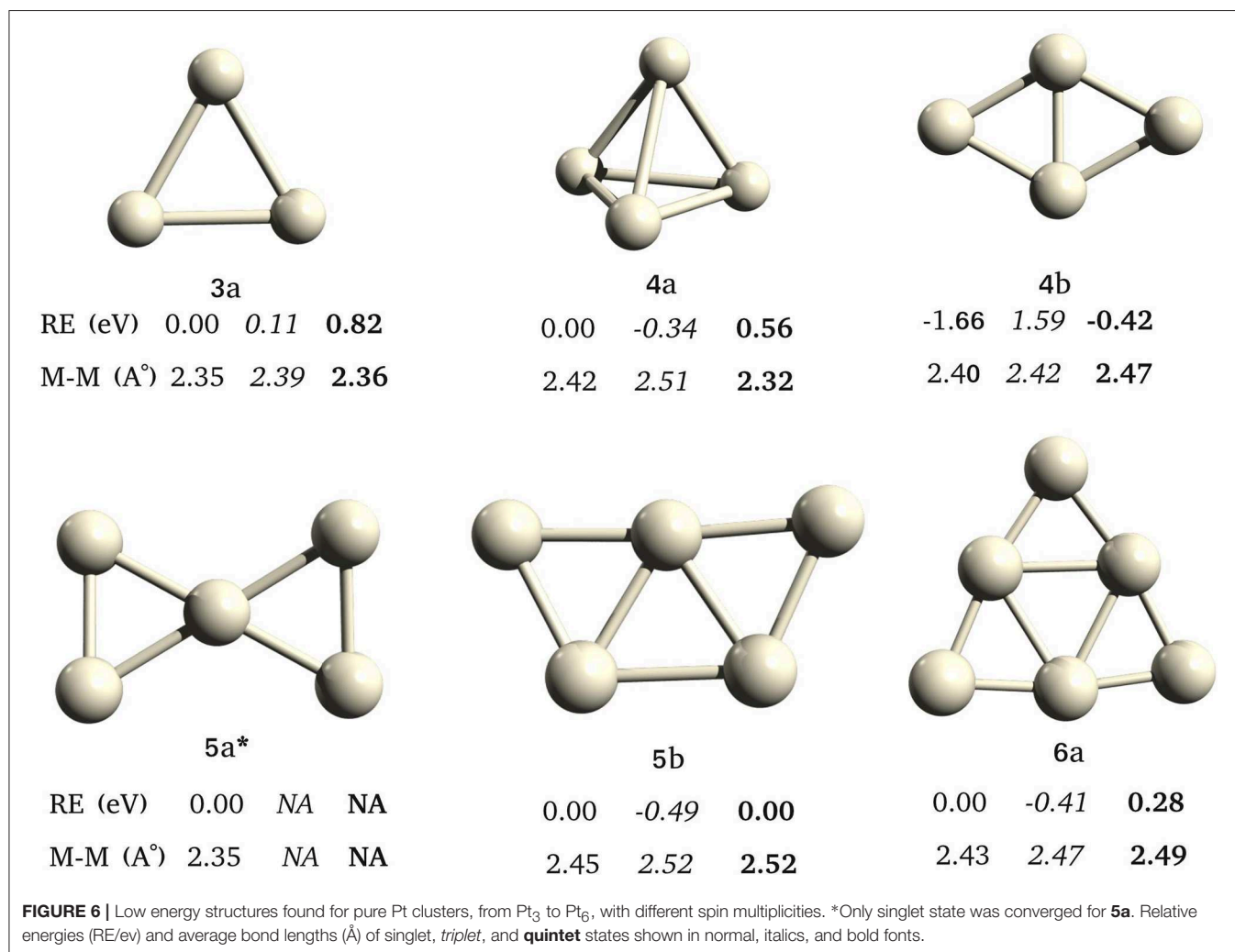
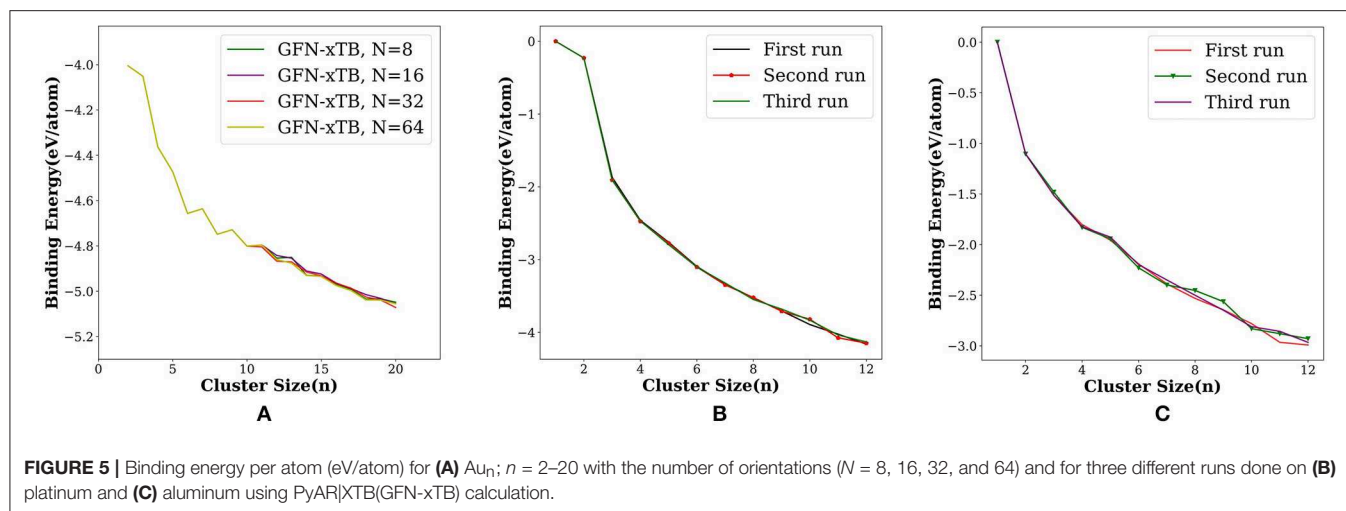
The search for global minimum using only eight orientations was able to locate the tetrahedral global minimum geometry of  $Au_{20}$ , however, not always. By varying the number of orientations in the search— $N = 8, 16, 32$ , and  $64$ —we checked the probability

of getting the global minimum. When the orientation number is 32, GM structure was found in a single run. As one can anticipate, the possible ways in which the new atom can be added to the  $(n - 1)^{th}$  cluster increases on increasing the cluster size. Therefore, we have to increase the number of orientation. With increasing cluster size. We have illustrated this by plotting the binding energy per atom for the runs with number of orientation as 8, 16, 32, and 64 (**Figure 5A**). We have made an option `auto` for the number of orientation  $N$  in which  $N$  doubles after each cycle starting with eight in the first cycle, then  $N$  increases as 16, 32, 64, 128, 256 and up to a maximum of 512.

#### 4.1.3. Platinum

We studied platinum nanoclusters as the next example as the Pt-based nanoclusters are useful materials with applications in various heterogeneous catalysis. Jennings and coworkers performed GA-DFT searches on small-sized ( $Pt_n$ ,  $n = 3-6$ ) platinum clusters to find their GM structures. The study showed that Pt clusters have non-singlet ground states, and the geometry of GM's can vary for different spin multiplicity (Jennings and Johnston, 2013). Thus, we have performed three different global minimum searches with multiplicities 1, 3, and 5 on  $Pt_n$ ;  $n = 3-6$  with PyAR|XTB.

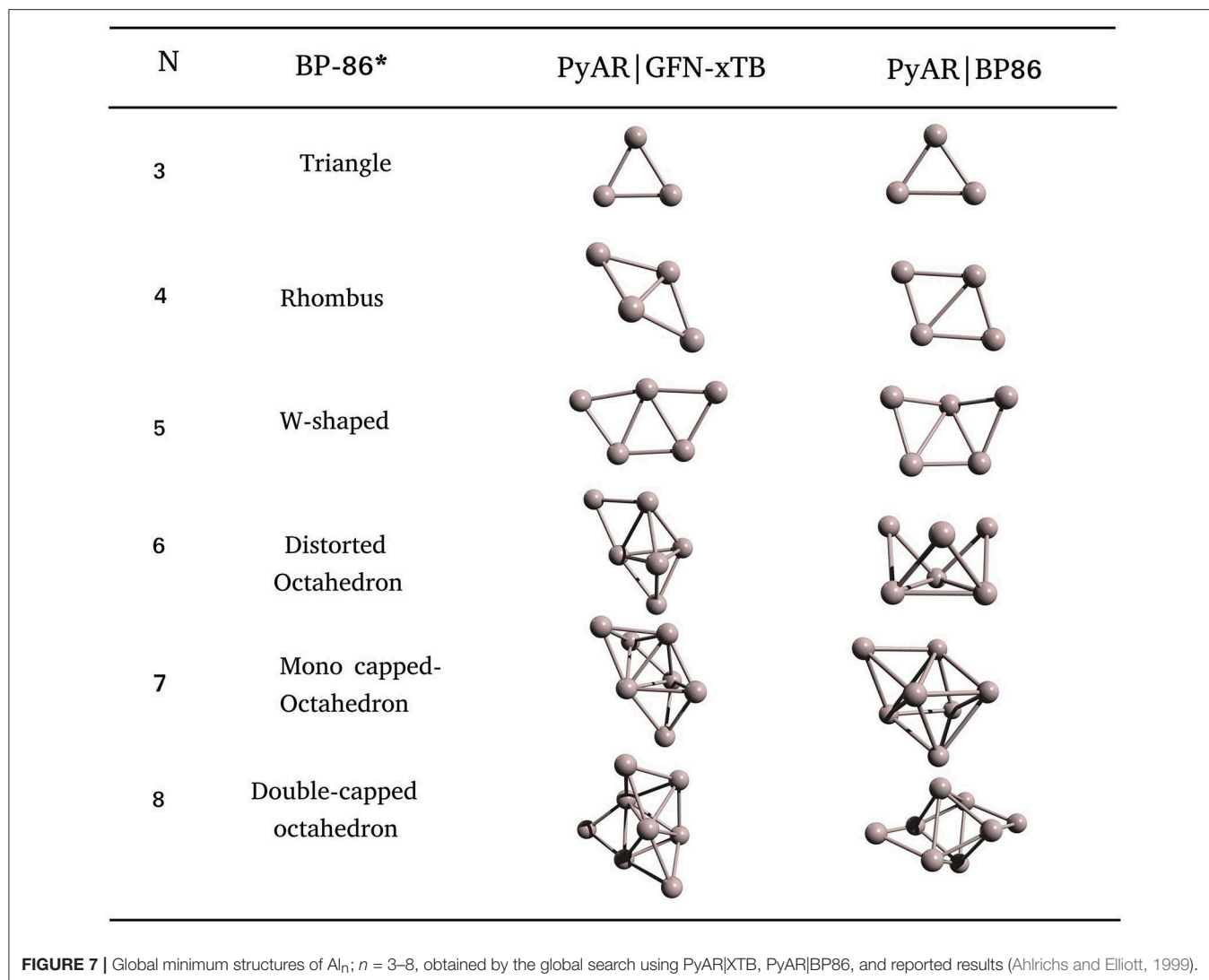
We have observed different global minima for different multiplicities (**Figure 6**) for  $Pt_4$  and  $Pt_5$ , in agreement with the GA-DFT study. The  $Pt_3$  has the same triangular geometry in singlet and triplet states, and singlet is the ground state. There are two geometries, **4a** and **4b** for  $Pt_4$ . The **4b** has the lowest energy in its singlet state. The ground state of **4a** is a triplet, however, it is higher in energy than the



singlet-**4b**. The **5a** is minima only in singlet state. The GM for  $Pt_5$  is **5b** in triplet state. The  $Pt_6$  has a triplet ground state (**5b**).

#### 4.1.4. Aluminum

The last example for the homometallic cluster in this article is the aluminum cluster. We have built the global minimum structures



of Al nanoclusters up to  $Al_{12}$  with PyAR|XTB, and up to  $Al_8$  with PyAR|BP86. There are several theoretical studies on Al clusters at various levels of theory, such as Sutton-Chen empirical potential (Joswig and Springborg, 2003), DFT (Ahlrichs and Elliott, 1999; Rao and Jena, 1999), and CCSD(T) (Shinde and Shukla, 2014; López-Estrada and Orgaz, 2015).

The most stable structure for the trimer,  $Al_3$  is triangular in both the calculations, PyAR|(XTB, BP86). The bent and linear isomers are 0.53 eV and 0.63 eV higher in energy compared to the most stable structure at BP86/def2-SVP level. We found a planar rhombus geometry for  $Al_4$  with PyAR|BP86 in agreement with the reported *ab initio* methods. PyAR|GFN-xTB calculation gave a slightly different non-planar rhombus geometry as the most stable structure, but tetrahedron is a minima at GA-Sutton Chen potential. The GM of  $Al_5$  is a planar W-shaped structure in our calculation (PyAR|(XTB, BP86)) in agreement with the reported minima from *ab initio* calculations.

The GM of  $Al_6$  by PyAR|XTB is a TBP with an edge-cap, but PyAR|BP86 calculation gave a crown-shaped structure as GM

(Figure 7). The structure of  $Al_6$  reported by Jones and Ahlrichs (Jones, 1993; Ahlrichs and Elliott, 1999) is a distorted octahedron, not in agreement with any of our minima. For  $Al_7$ , the trigonal bipyramid with two capped atoms is the GM at PyAR|XTB, while PyAR|BP86 produced a mono-capped octahedron that matched with the reported minima. The octamer  $Al_8$  showed capped trigonal bipyramid as the minima by PyAR|XTB, octahedral core with two edge-capped by PyAR|BP86 that matched with SC potential (Joswig and Springborg, 2003) and DFT studies (Jones, 1993; Ahlrichs and Elliott, 1999).

#### 4.1.5. General Features

We have studied various features of the approach to finding the global minima of metal nanoclusters. In gold and aluminum clusters, we have compared different methods. All the methods, including semiempirical, produced the same global minima for gold clusters, while the GM was highly dependent on the method for Al clusters. Hence, the choice of appropriate method is crucial.

Some of the clusters have different structural motifs for different sizes. Our method was able to capture the changes in the structural motifs. The global minima for gold clusters were flat upto the size of ten and were 3D geometries afterwards. In order to check these structural changes, we have carried out PyAR|XTB calculation on carbon clusters. We have observed minima corresponding to linear, monocyclic, tricyclic, and the bowl shapes (Figure S3).

We have checked the variation in binding energy per atom on varying the number of orientations ( $N$ ) in the Au cluster (Figure 5A). The use of more orientations was crucial, especially for the larger clusters. We have then checked the variation in BE for three separate runs for Pt and Al clusters. While the plot of BE for each run (Figure 5B) shows nearly perfect overlapping lines for Pt clusters, the BE's slightly differ for Al clusters (Figure 5C).

As the cluster size increases, the search space increases. Hence, either increase the  $N$ , or carry out multiple runs, to ensure that most of the local minima are found that increases the chance of finding the global minima. Between these two options, increasing  $N$  is better as the Tabu list ensures that the trial geometries are dissimilar, while multiple runs may end up in exploring the same local minima more often.

## 4.2. Binary Clusters

The mixing of two elements may result in properties that are different from the pure forms of each elemental clusters. In the case of binary clusters, we have to consider all different compositions between two elements. Here we have exhaustively explored all combinations in  $A_iB_j$ , where  $1 \leq i \leq m$ ;  $1 \leq j \leq n$ ;

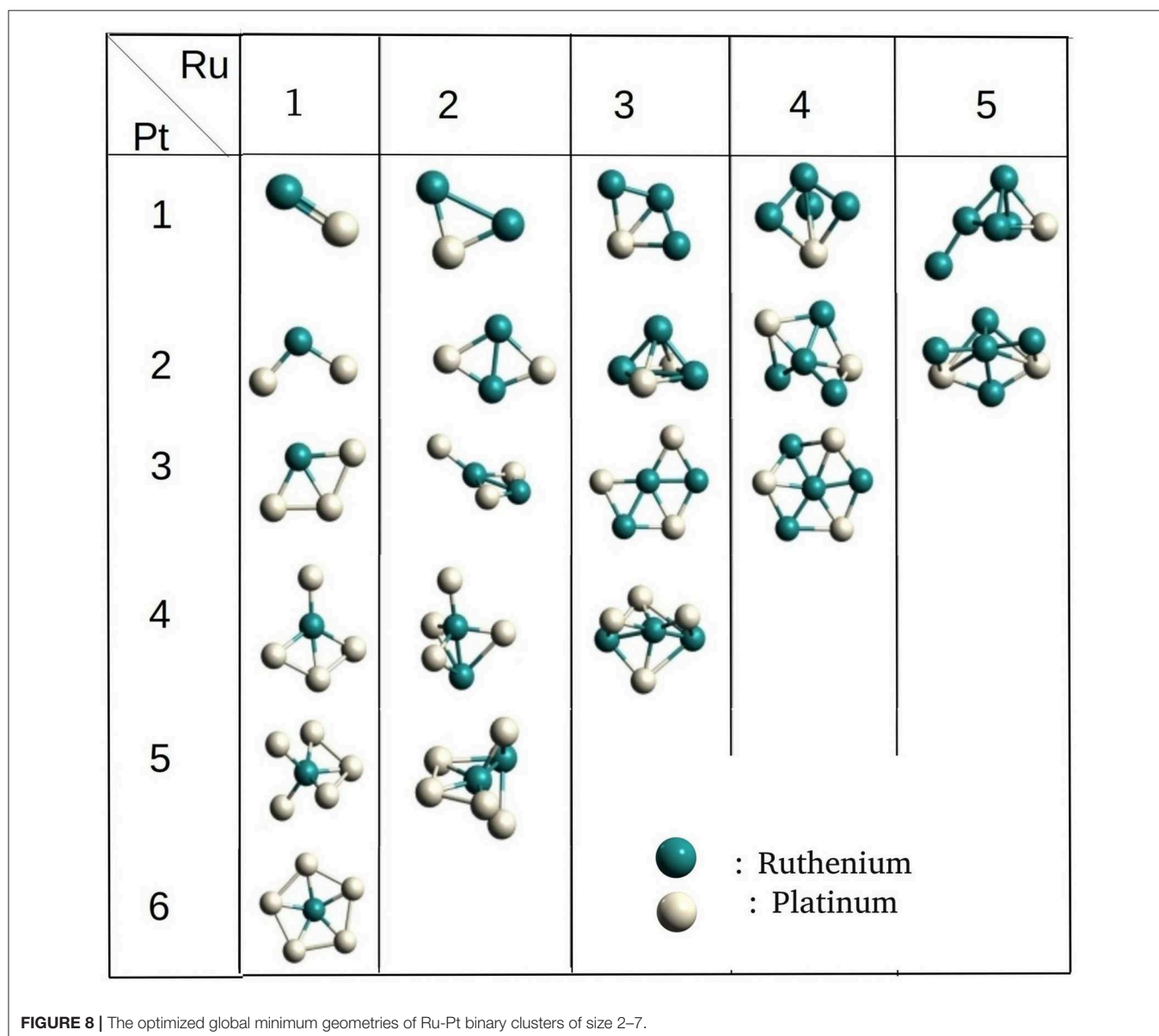
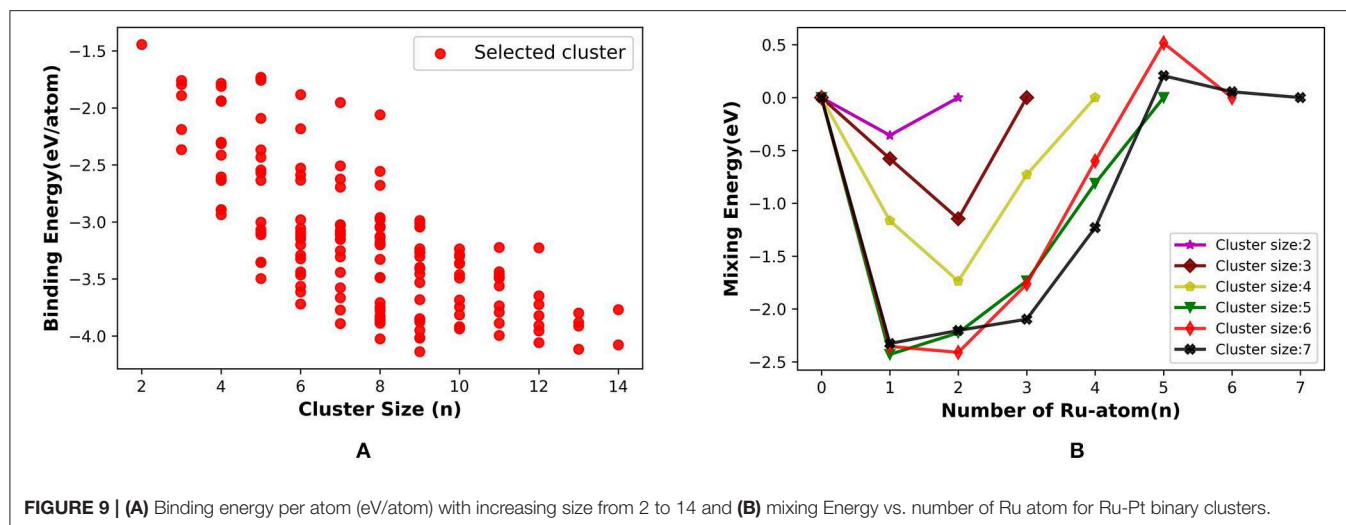


FIGURE 8 | The optimized global minimum geometries of Ru-Pt binary clusters of size 2–7.



**FIGURE 9 | (A)** Binding energy per atom (eV/atom) with increasing size from 2 to 14 and **(B)** mixing Energy vs. number of Ru atom for Ru-Pt binary clusters.

the cluster size  $N = m + n$ , for ruthenium-platinum and gold-platinum binary clusters. One notable feature in the geometries is that, one of the elements tends to become part of the core, while the other tends to be on the surface. The other property of interest is the mixing energy that shows the stability of binary clusters compared to that of the pure unary clusters.

#### 4.2.1. Ruthenium-Platinum Binary Clusters

The binary Ru-Pt nanoalloys showed remarkable enhancement in catalytic activity for CO oxidation (Arico et al., 2001; Liu et al., 2006), compared to when platinum is used in its pure form as a catalyst (Bion et al., 2008), and avoids some of the drawbacks. We applied our method for building binary clusters implemented in `binary_aggregator` in PyAR to build Ru-Pt binary system with the interface to XTb program using GFN-xTB method. We built the Ru-Pt binary clusters up to a total cluster size of 14, i.e., Ru<sub>1</sub>Pt<sub>1</sub> ... Ru<sub>7</sub>Pt<sub>7</sub>. The lowest energetic clusters are shown in Figure 8 for a size of 2 to 7.

The general features of the GM geometries match with the reported trend (Demiroglu et al., 2017). In general, the Ru prefers to occupy the core of the clusters with the maximum number of bonds. The Pt, on the other hand, minimizes its number of bonds by seeping on to the surface, having at most three bonds. This observation is in accordance with the higher cohesive energy of Ru (6.74 eV) compared to Pt. (5.84 eV) (Kittel, 2005). The binding energy of the Ru<sub>2</sub> dimer is lower than that of Pt<sub>2</sub>, 2.00 eV and 1.94 eV, and the Ru-Pt has the higher binding energy than both (2.13 eV) (Demiroglu et al., 2017). The GM geometries from PyAR|XTb maintain these qualitative features although the individual structures are not identical with the reported structures from Demiroglu et al., as most of these geometries have high spin ground states and we have considered only singlet states (Demiroglu et al., 2017).

For the cluster size of four, all the combinations of (Ru,Pt)<sub>4</sub> have similar, non-planar bitriangular geometries. Ru-Ru bond is shorter in Ru<sub>2</sub>Pt<sub>2</sub>, but two Pt atoms prefer to stay away from each other. For cluster size higher than four, the geometry of GM changes with composition. As the composition of Ru increases

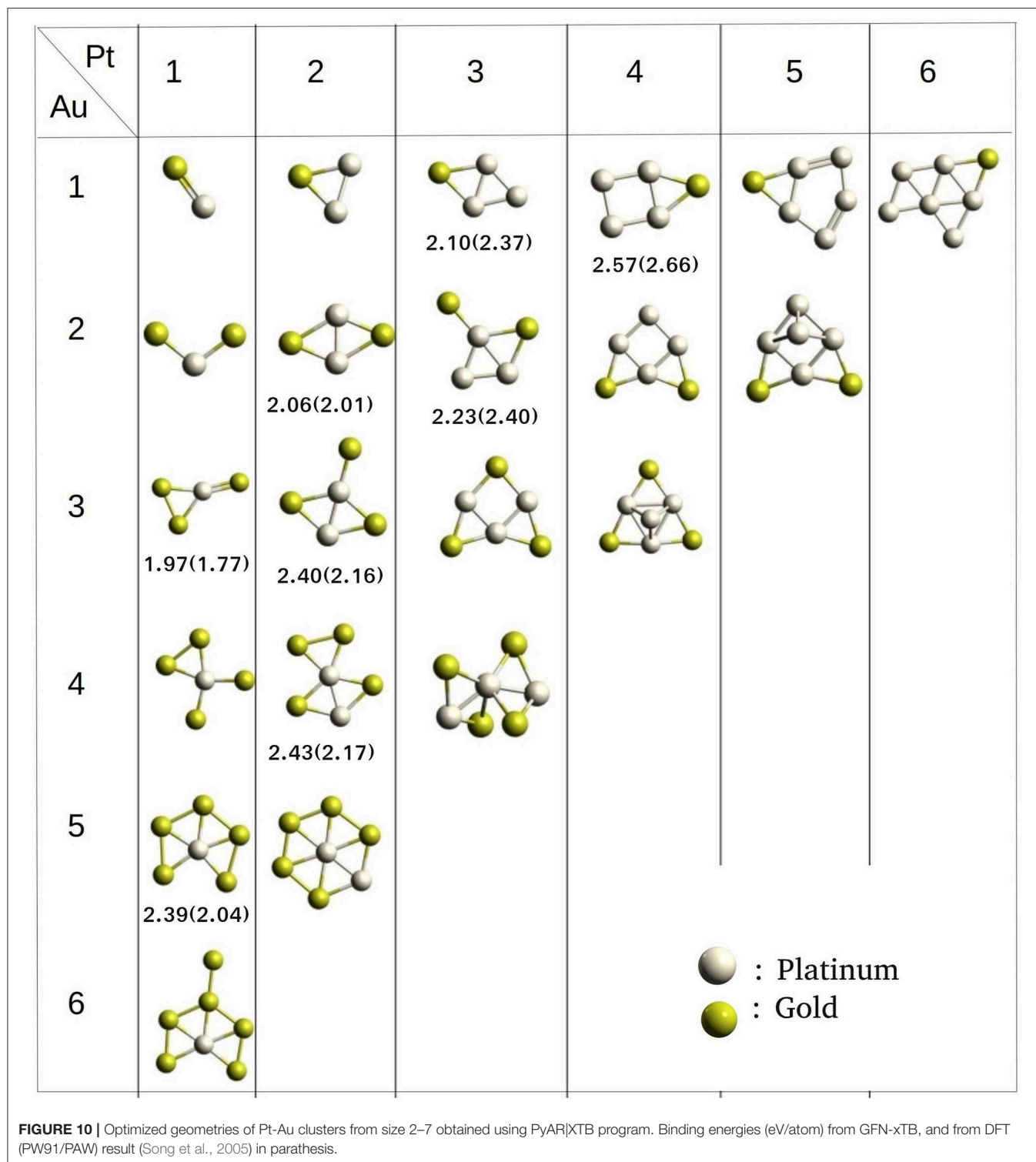
in (Ru, Pt)<sub>5</sub>, the structure changes from planar to 3-D. Similar planar structures were found for Ru<sub>1</sub>Pt<sub>4</sub> and Ru<sub>2</sub>Pt<sub>3</sub>. For cluster sizes with six and seven atoms also, the clusters with a higher composition of Ru have 3-D structures.

The binding energy per atom increases with the cluster size for (Ru, Pt)<sub>N</sub> binary cluster in the range that we have considered, up to total cluster size 14. Figure 9A shows the average binding energy vs. cluster size of the Ru-Pt clusters, which includes all the selected unique isomers along with GM. The highest BE for each cluster size increases as the cluster grows and gains the highest stability at nine and then again at 13. Our semi-empirical results are in qualitative agreement with the reported DFT results (Demiroglu et al., 2017).

We have calculated the mixing energy ( $\delta$ ), the excess energy of nanoalloy over the pure cluster of the same size, for RuPt binary clusters of size  $N = m + n = 2-7$ . The effect of mixing Ru with Pt in small clusters calculated as a function of Ru atoms for all compositions of Ru<sub>m</sub>Pt<sub>n</sub> from  $2 \leq N \leq 7$  clusters are plotted in Figure 9B. The mixing is favorable when  $\delta$  is negative. In our calculation, mixed clusters are more stabilized than the pure clusters except for Ru<sub>5</sub>Pt<sub>1</sub> and Ru<sub>5</sub>Pt<sub>2</sub>. The DFT calculation by Demiroglu et al. (2017), on the other hand, shown positive mixing energy for Ru<sub>3</sub>Pt<sub>1</sub>. Ru-Pt diatomic molecule is more stable than the pure Ru<sub>2</sub> or Pt<sub>2</sub> dimer. The clusters with one Ru atom (Ru<sub>1</sub>Pt<sub>N</sub>) more stable than the other possible combinations for  $N = 2, 5$ , and 7. Two Ru atoms made the binary clusters more feasible when  $N = 3, 4$ , and 6. Therefore, (Ru, Pt)<sub>N</sub> binary clusters with a lesser composition of Ru atoms (one or two) are more favorable in our calculation using semi-empirical method (PyAR|GFN-xTB).

#### 4.2.2. Platinum-Gold Binary Clusters

Platinum-Gold nanoalloys are one of the most studied binary clusters because of their catalytic properties, for example, as a catalyst for CO adsorption (Logsdail et al., 2009; Kaizuka et al., 2010). Song et al. have studied the bonding properties of CO on Pt-Au binary clusters (Song et al., 2005). The catalytic activity of a cluster largely depends on the electronic properties. By



introducing gold atom in the pure platinum cluster, the electronic properties and thereby, catalytic activity is enhanced.

We have built the  $(\text{Pt}, \text{Au})_N$  binary clusters;  $N = 2-14$  using PyAR|XTB. The lowest energy structures of  $N = 2-7$  are shown in **Figure 10**. For  $(\text{Pt}, \text{Au})_3$  cluster, the  $\text{Pt}_2\text{Au}$  has a triangular

geometry with Pt-Pt and Pt-Au bonds, while the  $\text{PtAu}_2$  has a bent structure with both the Au atoms bonded to Pt and has long Au-Au distance.  $\text{PtAu}_3$  has a planar structure with a triangle of  $\text{PtAu}_2$  and an exocyclic Au attached to Pt. The other  $(\text{Pt}, \text{Au})_4$  structures,  $\text{Pt}_2\text{Au}_2$  and  $\text{Pt}_3\text{Au}_1$  has similar bicyclic

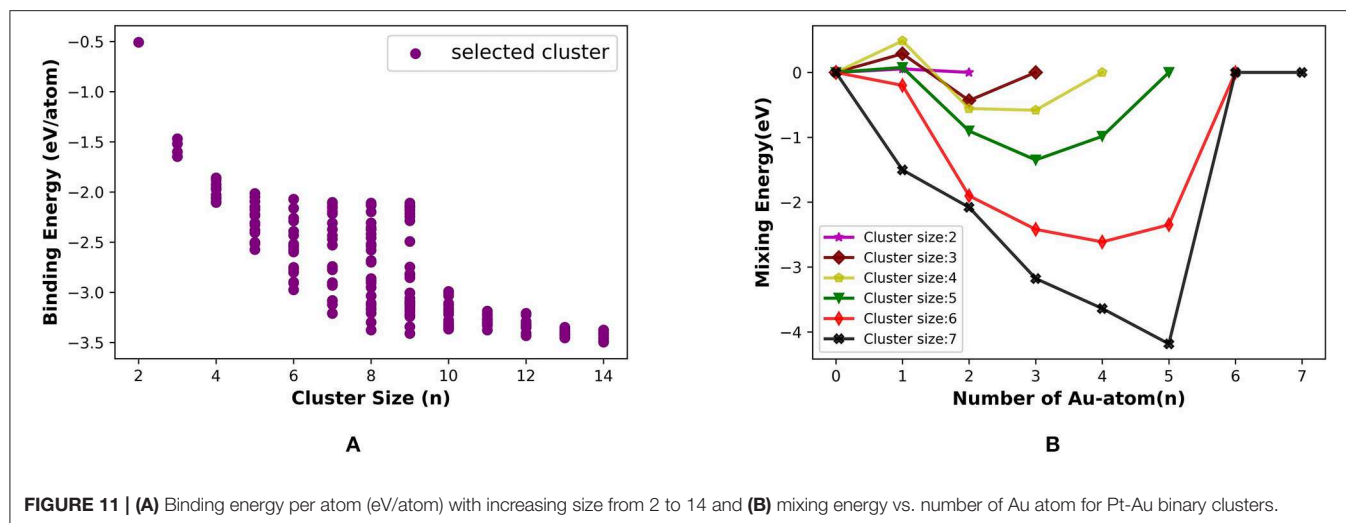


**FIGURE 11 | (A)** Binding energy per atom (eV/atom) with increasing size from 2 to 14 and **(B)** mixing energy vs. number of Au atom for Pt-Au binary clusters.

quasi-planar structures. Among the  $(\text{Pt,Au})_5$  clusters,  $\text{Au}_2\text{Pt}_3$  and  $\text{Au}_3\text{Pt}_2$  where the composition of either gold or platinum is 60% have similar geometries as GM. The  $(\text{Pt,Au})_5$  with 80% gold composition makes the structure having a triangular base, but the higher percentage of platinum changes the geometry to a fused four-and-three-membered rings.

As the cluster grows in size, the composition of the alloy will show significant effects on the structure and other properties. For cluster sizes of six and seven atoms, the structures with a higher composition of gold prefer to form planar-like structure. When the composition of Pt is maximum, the cluster tends to acquire a 3D geometry. While Au occupies external sites, Pt occupies the core sites. Apart from these general features, the GM geometries from our study do not match well with the global minimum geometries reported in the literature (Song et al., 2005), due to the different level of theory applied (GFN-xTB vs PW91/PAW) for studying the clusters.

We estimated the average binding energy for  $(\text{Pt, Au})_N$  clusters ( $N = 2-14$ ) using PyAR|GFN-xTB. The cluster gains the highest stability when it reaches the size nine and again at size 14 in **Figure 11A**. We compared our results (PyAR|XTB) with the DFT results by Song et al. (2005). Binding energies of planar  $\text{Pt}_1\text{Au}_3$ ,  $\text{Pt}_2\text{Au}_2$ , and  $\text{Pt}_3\text{Au}_1$  are shown in 10 with the corresponding reported values. The planar minima of  $\text{Pt}_4\text{Au}_1$ ,  $\text{Pt}_3\text{Au}_2$ , and  $\text{Pt}_2\text{Au}_3$  are in agreement with the reported geometries.

We have calculated the mixing energy—the stability of mixed cluster compared to its pure form—for the  $(\text{Pt, Au})_N$  clusters. Most of the GM geometries with combinations of  $\text{Pt}_m\text{Au}_n$  ( $2 \leq m + n \leq 7$ ) clusters have negative mixing energy, except for  $\text{Pt}_1\text{Au}_2$ ,  $\text{Pt}_1\text{Au}_3$  (**Figure 11B**). Hence, the mixing is, in general, favorable. For cluster size up to seven, the clusters with one or two Pt atoms have the highest stability.

### 4.3. Ternary Aggregate

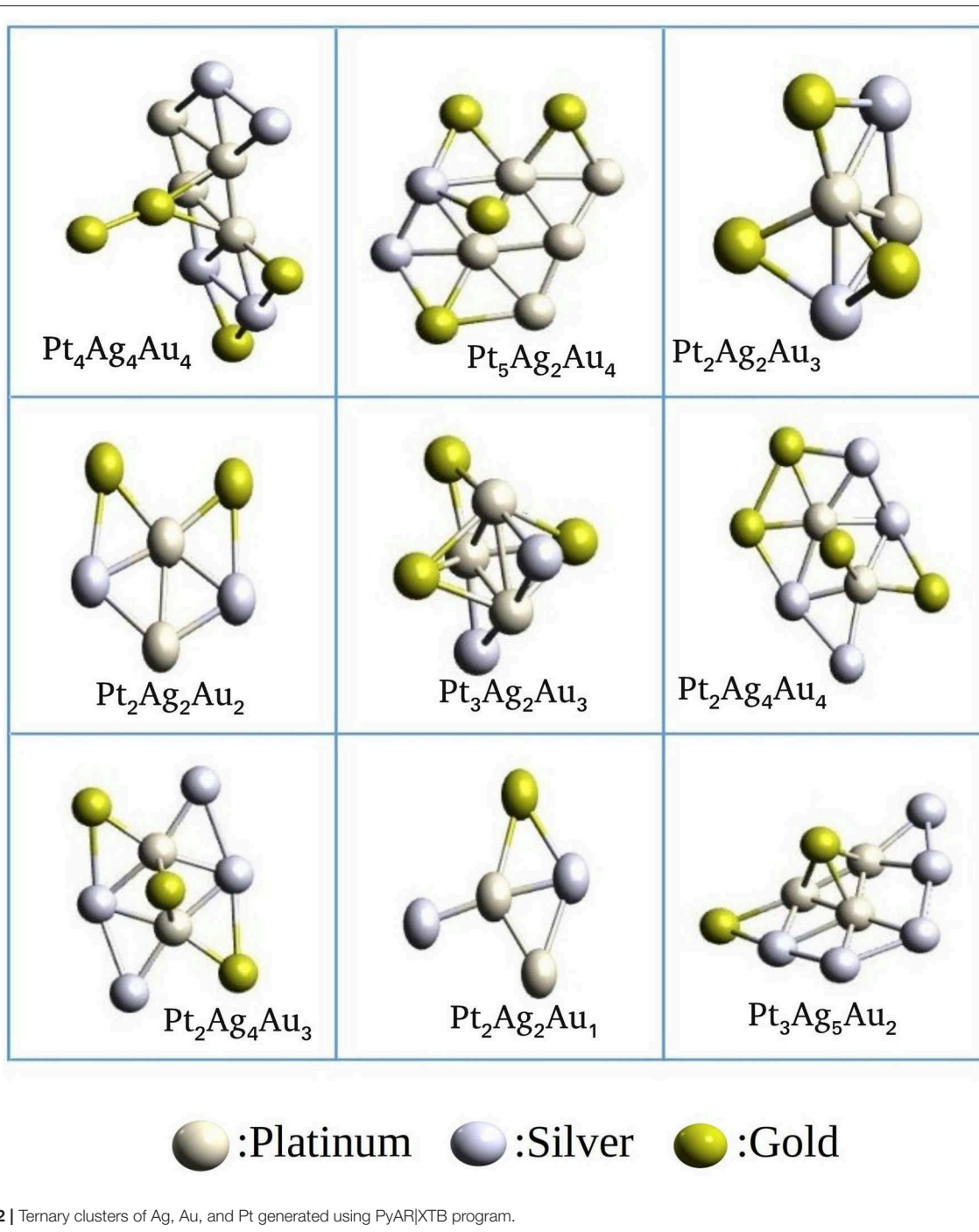
The catalytic activity of metal nanoclusters can be enhanced by introducing a second element as well as a third element. Some ternary metal clusters were shown to have higher activity than

their unary or binary counterparts (Fang et al., 2011). However, the details of the mechanisms for the enhanced activity is largely unknown as even the structural details of these binary, ternary or other heterometallic clusters are unknown. Finding the global minima of the ternary cluster is even more difficult as compared to the unary and binary systems. Ternary cluster,  $\text{A}_l\text{B}_m\text{C}_n$  ( $l + m + n = N$ ), can have geometries different from their unary or binary counterparts and can have different structures for different compositions. This high level of complexity in the PES is a challenge for the high-level theoretical calculations to explore the surfaces efficiently. There is a lot to be learnt about the ternary clusters; computational chemistry can serve greatly in this endeavor.

We have studied Platinum-Gold-Silver clusters as an example for a ternary system to validate the `ternary_aggregator` module implemented in PyAR program. We have built the Pt-Ag-Au cluster of total size up to 15 using xTB interface. In the GM geometries, Pt and Ag are near the core, while Au atoms are in the periphery. As we have discussed in the binary systems, these preferences can be attributed to the bond strengths. The bond strength calculated at GFN-xTB level follows the order:  $\text{Ag-Ag} (-5.19 \text{ eV}) > \text{Pt-Pt} (-4.4 \text{ eV}) > \text{Au-Au} (-3.9 \text{ eV})$ ; the bond energy is given in parenthesis. The geometries of the most stable ternary clusters are shown in **Figure 12**. Most of the structures are quasi-planar or three-dimensional. The general features of the minima are in accordance with the studies by Pacheco-Contreras et al. using Basin Hopping global search with Gupta Potential (as the force field), and using DFT for final optimization for more accuracy (Pacheco-Contreras et al., 2018).

## 5. CONCLUSIONS

We have developed a methodology to build the unique geometries of nanoclusters and nanoalloys. The clusters are built by adding atoms one-by-one starting from one atom up to the desired size. The following steps are involved in the method: (a) For adding an atom to the  $N$ -sized cluster,



several trial orientations are generated by placing the atom at different random positions around the cluster, (b) These orientations are then optimized by gradient-based methods by the interfaced electronic structure programs, (c) From all the optimized geometries, the similar geometries are removed, the unique structures are selected by clustering algorithms, and these selected geometries are used for the next cycle. These steps (a–c) are repeated to add an atom to all the selected seed

molecules. These atoms are added until the cluster grows to the desired size. The similarity between the molecules are compared using the molecular representation based on fingerprints of the Coulomb matrix.

We studied nanoclusters of palladium, gold, platinum, and aluminum, binary clusters of Ru-Pt and Au-Pt, and ternary clusters of Ag-Au-Pt. The method is shown to produce all the reported global minimum structures, along with other minima,

when we used the same or similar electronic structure methods and the same spin-states. Differences were seen when we used the semiempirical GFN-xTB method to compare the reported structure and properties from DFT or CCSD(T) studies. We have also evaluated some popular properties such as binding energy per atom, mixing energy, and compared with the reported ones.

We have varied some of the parameters in our approach for comparison of efficiency in finding the global minima and other properties of metal nanoclusters. We have compared different electronic structure methods, semiempirical and a few DFT functionals, in gold and aluminum clusters. While all the methods produced the same global minima for gold clusters, the geometries of maximum stability were highly dependent on the method for Al clusters. The method dependency was also seen in identifying the ground spin-state in Pt clusters. Thus, we can use less expensive methods such as semiempirical methods or empirical potentials for the clusters which do not change the ground-state multiplicity, and for which these methods give good results comparable to high-level *ab initio* or DFT methods. We can also use a two-layer approach where the initial search is done by cheaper methods, and the selected geometries can be optimized at a higher level.

We checked the effect of varying the number of orientations by comparing the binding energy per atom in the Au clusters. The study showed that as the cluster size increase more orientations has to be used for better results. In the same way, the result from different runs may vary if a small number of orientations are used, as was found by comparing the BE for three separate runs for Pt and Al clusters. As the cluster size increases, the search space increases and hence either number of orientations has to be increased or multiple runs have to be carried out to ensure that most of the local minima are found to increase the chance of finding the global minima.

A major potential challenge in such cluster-growing methods is the ability to capture the changes in structural motifs. We have seen that the GM's in Au<sub>n</sub> clusters changed from 2D to 3D on going from  $n = 10$ –11. We also found similar structural changes

in carbon clusters, 1D linear geometry, to 2D ring structures, and 3D structures including bowl-shaped geometries.

Thus, by building the cluster of size  $n$  by exploring three degrees of freedom involving the relative orientations of  $n - 1$  and one atom gives the minima obtained by exploring 3N-6 degrees of freedom by the other methods. The direct comparison of complexity for the  $n$ -sized cluster is not meaningful because we have to add the complexity for exploring each of the clusters of size up to  $n$ . The major limitation our method is that it can be more expensive for building a cluster of a particular size of  $n$  as the method has to build all the clusters from size 2 to  $n$ . This method may not be very useful if one is only interested in only the  $n$ -sized cluster. Our method, however, is useful for studying the evolution of properties with growing cluster size.

## DATA AVAILABILITY STATEMENT

All datasets generated for this study are included in the manuscript/**Supplementary Files**.

## AUTHOR CONTRIBUTIONS

AA designed the project. MK and RM did the calculations. All the authors contributed to the manuscript preparation.

## ACKNOWLEDGMENTS

We thank the Department of Science and Technology (DST), New Delhi, India for the FIST grants (SR/FST/CSII-026/2013 and SR/FST/CSII-011/2005) and IIT Kharagpur for computational facilities. MK thank DST for INSPIRE fellowship.

## SUPPLEMENTARY MATERIAL

The Supplementary Material for this article can be found online at: <https://www.frontiersin.org/articles/10.3389/fchem.2019.00644/full#supplementary-material>

## REFERENCES

- Adamo, C., and Barone, V. (1999). Toward reliable density functional methods without adjustable parameters: the PBE0 model. *J. Chem. Phys.* 110, 6158–6170. doi: 10.1063/1.478522
- Ahlich, R., and Elliott, S. D. (1999). Clusters of aluminum, a density functional study. *Phys. Chem. Chem. Phys.* 1, 13–21. doi: 10.1039/a807713d
- Anoop, A. (2019). *Pyar*. Available online at: <https://github.com/anooplab/pyar>
- Arico, A., Srinivasan, S., and Antonucci, V. (2001). Dmfc: from fundamental aspects to technology development. *Fuel Cells* 1, 133–161.
- Assadollahzadeh, B., and Schwerdtfeger, P. (2009). A systematic search for minimum structures of small gold clusters aun ( $n=2$ -20) and their electronic properties. *J. Chem. Phys.* 131:064306. doi: 10.1063/1.3204488
- Baek, H., Moon, J., and Kim, J. (2017). Benchmark study of density functional theory for neutral gold clusters, aun ( $n = 2$ -8). *J. Phys. Chem. A* 121, 2410–2419. doi: 10.1021/acs.jpca.6b11868
- Balasubramanian, K. (1989). Ten low-lying electronic states of pd<sub>3</sub>. *J. Chem. Phys.* 91, 307–313. doi: 10.1063/1.457518
- Baletto, F., and Ferrando, R. (2005). Structural properties of nanoclusters: energetic, thermodynamic, and kinetic effects. *Rev. Mod. Phys.* 77, 371–423. doi: 10.1103/RevModPhys.77.371
- Barbati, M., Bruno, G., and Genovese, A. (2012). Applications of agent-based models for optimization problems: a literature review. *Exp. Syst. Appl.* 39, 6020–6028. doi: 10.1016/j.eswa.2011.12.015
- Becke, A. D. (1988). Density-functional exchange-energy approximation with correct asymptotic behavior. *Phys. Rev. A* 38, 3098–3100. doi: 10.1103/PhysRevA.38.3098
- Bion, N., Epron, F., Moreno, M., Marino, F., and Duprez, D. (2008). Preferential oxidation of carbon monoxide in the presence of hydrogen (prox) over noble metals and transition metal oxides: advantages and drawbacks. *Top. Catal.* 51:76. doi: 10.1007/s11244-008-9116-x
- Bishea, G. A., and Morse, M. D. (1991). Spectroscopic studies of jet-cooled agau and au<sub>2</sub>. *J. Chem. Phys.* 95, 5646–5659. doi: 10.1063/1.461639
- Dai, D., and Balasubramanian, K. (1995). Electronic structures of pd<sub>4</sub> and pt<sub>4</sub>. *J. Chem. Phys.* 103, 648–655. doi: 10.1063/1.470098
- Davis, J. B. A., Shayeghi, A., Horswell, S. L., and Johnston, R. L. (2015). The birmingham parallel genetic algorithm and its application to the direct DFT global optimisation of IrN( $n = 10$ –20) clusters. *Nanoscale* 7, 14032–14038. doi: 10.1039/C5NR03774C
- Demiroglu, I., Yao, K., Hussein, H. A., and Johnston, R. L. (2017). Dft global optimization of gas-phase subnanometer ru–pt clusters. *J. Phys. Chem. C* 121, 10773–10780. doi: 10.1021/acs.jpcc.6b11329

- Doye, J. P. K., and Wales, D. J. (1998). Thermodynamics of global optimization. *Phys. Rev. Lett.* 80, 1357–1360. doi: 10.1103/PhysRevLett.80.1357
- Eberhardt, W. (2002). Clusters as new materials. *Surf. Sci.* 500, 242–270. doi: 10.1016/S0039-6028(01)01564-3
- Edwards, P. P., Johnston, R. L., Rao, C. N. R., Tunstall, D. P., and Johnston, R. L. (1998). The development of metallic behaviour in clusters. *Philos. Trans. R. Soc. Lond. Ser. A* 356, 211–230. doi: 10.1098/rsta.1998.0158
- Fang, P.-P., Duan, S., Lin, X.-D., Anema, J. R., Li, J.-F., Buriez, O., et al. (2011). Tailoring au-core pd-shell pt-cluster nanoparticles for enhanced electrocatalytic activity. *Chem. Sci.* 2, 531–539. doi: 10.1039/C0SC00489H
- Floudas, C. A., and Gounaris, C. E. (2008). A review of recent advances in global optimization. *J. Glob. Optim.* 45:3. doi: 10.1007/s10898-008-9332-8
- Frisch, M., Trucks, G., Schlegel, H., Scuseria, G., Robb, M., Cheeseman, J., et al. (2016). *Gaussian 16. Revision A 3*.
- Furche, F., Ahlrichs, R., Hättig, C., Klopper, W., Sierka, M., and Weigend, F. (2014). Turbomole. *Wiley Interdiscip. Rev.* 4, 91–100. doi: 10.1002/wcms.1162
- Glover, F. (1986). Future paths for integer programming and links to artificial intelligence. *Comput. Operat. Res.* 13, 533–549. doi: 10.1016/0305-0548(86)90048-1
- Glover, F. (1989). Tabu search—part i. *ORSA J. Comput.* 1, 190–206. doi: 10.1287/ijoc.1.3.190
- Glover, F. (1990). Tabu search—part II. *ORSA J. Comput.* 2, 4–32. doi: 10.1287/ijoc.2.1.4
- Götz, D. A., Schäfer, R., and Schwerdtfeger, P. (2013). The performance of density functional and wavefunction-based methods for 2d and 3d structures of au10. *J. Comput. Chem.* 34, 1975–1981. doi: 10.1002/jcc.23338
- Götz, D. A., Shayeghi, A., Johnston, R. L., Schwerdtfeger, P., and Schäfer, R. (2016). Structural evolution and metallicity of lead clusters. *Nanoscale* 8, 11153–11160. doi: 10.1039/C6NR02080A
- Grimme, S., Bannwarth, C., and Shushkov, P. (2017). A robust and accurate tight-binding quantum chemical method for structures, vibrational frequencies, and noncovalent interactions of large molecular systems parametrized for all spd-block elements ( $z = 1-86$ ). *J. Chem. Theory Comput.* 13, 1989–2009. doi: 10.1021/acs.jctc.7b00118
- Grimme, S., Ehrlich, S., and Goerigk, L. (2011). Effect of the damping function in dispersion corrected density functional theory. *J. Comput. Chem.* 32, 1456–1465. doi: 10.1002/jcc.21759
- Gruene, P., Rayner, D. M., Redlich, B., van der Meer, A. F., Lyon, J. T., Meijer, G., et al. (2008). Structures of neutral au7, au19, and au20 clusters in the gas phase. *Science* 321, 674–676. doi: 10.1126/science.1161166
- Heiles, S., and Johnston, R. L. (2013). Global optimization of clusters using electronic structure methods. *Int. J. Quant. Chem.* 113, 2091–2109. doi: 10.1002/qua.24462
- Jäger, M., Schäfer, R., and Johnston, R. L. (2018). First principles global optimization of metal clusters and nanoalloys. *Adv. Phys. X* 3:1516514. doi: 10.1080/23746149.2018.1516514
- James, A., Kowalczyk, P., Simard, B., Pinegar, J., and Morse, M. (1994). The  $a1u \leftarrow x0+g$  system of gold dimer. *J. Mol. Spectrosc.* 168, 248–257. doi: 10.1006/jmsp.1994.1275
- Jennings, P., and Johnston, R. (2013). Structures of small ti- and v-doped pt clusters: a GA-DFT study. *Comput. Theoret. Chem.* 1021, 91–100. doi: 10.1016/j.comptc.2013.06.033
- Johnston, R. L. (2002). *Atomic and Molecular Clusters*. London: CRC Press.
- Johnston, R. L. (2003). Evolving better nanoparticles: genetic algorithms for optimising cluster geometries. *Dalton Trans.* 2003, 4193–4207. doi: 10.1039/b305686d
- Jones, R. (1993). Simulated annealing study of neutral and charged clusters: Al n and ga n. *J. Chem. Phys.* 99, 1194–1206. doi: 10.1063/1.465363
- Jortner, J. (1992). Cluster size effects. *Zeitschrift für Physik D Atoms Molecules Clusters* 24, 247–275. doi: 10.1007/BF01425749
- Joswig, J.-O., and Springborg, M. (2003). Genetic-algorithms search for global minima of aluminum clusters using a sutton-chen potential. *Phys. Rev. B* 68:085408. doi: 10.1103/PhysRevB.68.085408
- Kaizuka, K., Miyamura, H., and Kobayashi, S. (2010). Remarkable effect of bimetallic nanocluster catalysts for aerobic oxidation of alcohols: combining metals changes the activities and the reaction pathways to aldehydes/carboxylic acids or esters. *J. Am. Chem. Soc.* 132, 15096–15098. doi: 10.1021/ja108256h
- Khare, A., and Rangnekar, S. (2013). A review of particle swarm optimization and its applications in solar photovoltaic system. *Appl. Soft Comput.* 13, 2997–3006. doi: 10.1016/j.asoc.2012.11.033
- Kirkpatrick, S., Gelatt, C. D., and Vecchi, M. P. (1983). Optimization by simulated annealing. *Science* 220, 671–680. doi: 10.1126/science.220.4598.671
- Kittel, C. (2005). *Introduction to Solid State Physics*. New York, NY: John Wiley & Sons.
- Lin, S.-S., Strauss, B., and Kant, A. (1969). Dissociation energy of pd2. *J. Chem. Phys.* 51, 2282–2283. doi: 10.1063/1.1672334
- Liu, H., Song, C., Zhang, L., Zhang, J., Wang, H., and Wilkinson, D. P. (2006). A review of anode catalysis in the direct methanol fuel cell. *J. Power Sour.* 155, 95–110. doi: 10.1016/j.jpowsour.2006.01.030
- Logsdail, A., Paz-Borbón, L. O., and Johnston, R. L. (2009). Structures and stabilities of platinum–gold nanoclusters. *J. Comput. Theor. Nanosci.* 6, 857–866. doi: 10.1166/jctn.2009.1118
- López-Estrada, O. and Orgaz, E. (2015). Theoretical study of the spin competition in small-sized al clusters. *J. Phys. Chem. A* 119, 11941–11948. doi: 10.1021/acs.jpca.5b09871
- Lv, J., Wang, Y., Zhu, L., and Ma, Y. (2012). Particle-swarm structure prediction on clusters. *J. Chem. Phys.* 137:084104. doi: 10.1063/1.4746757
- Nandi, S., Bhattacharyya, D., and Anoop, A. (2018). Prebiotic chemistry of HCN tetramerization by automated reaction search. *Chemistry* 24, 4885–4894. doi: 10.1002/chem.201705492
- Nandi, S., McAnanama-Breton, S. R., Waller, M. P., and Anoop, A. (2017). A tabu-search based strategy for modeling molecular aggregates and binary reactions. *Comput. Theor. Chem.* 1111, 69–81. doi: 10.1016/j.comptc.2017.03.040
- Nava, P., Sierka, M., and Ahlrichs, R. (2003). Density functional study of palladium clusters. *Phys. Chem. Chem. Phys.* 5, 3372–3381. doi: 10.1039/B303347C
- Neese, F. (2018). Software update: the orca program system, version 4.0. *Wiley Interdiscip. Rev.* 8:e1327. doi: 10.1002/wcms.1327
- Pacheco-Contreras, R., Juárez-Sánchez, J. O., Dessens-Félix, M., Aguilera-Granja, F., Fortunelli, A., and Posada-Amarillas, A. (2018). Empirical-potential global minima and dft local minima of trimetallic aglaupmtn ( $1+ m+ n= 13, 19, 33, 38$ ) clusters. *Comput. Mater. Sci.* 141, 30–40. doi: 10.1016/j.commatsci.2017.09.022
- Pedregosa, F., Varoquaux, G., Gramfort, A., Michel, V., Thirion, B., Grisel, O., et al. (2011). Scikit-learn: machine learning in Python. *J. Mach. Learn. Res.* 12, 2825–2830. Available online at: <http://jmlr.csail.mit.edu/papers/v12/pedregosa11a.html>
- Perdew, J. P. (1986). Density-functional approximation for the correlation energy of the inhomogeneous electron gas. *Phys. Rev. B* 33, 8822–8824. doi: 10.1103/PhysRevB.33.8822
- Pettersson, L. G., Wahlgren, U., and Gropen, O. (1983). Effective core potential calculations using frozen orbitals. applications to transition metals. *Chem. Phys.* 80, 7–16. doi: 10.1016/0301-0104(83)85164-7
- Rao, B. K., and Jena, P. (1999). Evolution of the electronic structure and properties of neutral and charged aluminum clusters: a comprehensive analysis. *J. Chem. Phys.* 111, 1890–1904. doi: 10.1063/1.479458
- Reveles, J. U., Köster, A. M., Calaminici, P., and Khanna, S. N. (2012). Structural changes of pd13 upon charging and oxidation/reduction. *J. Chem. Phys.* 136:114505. doi: 10.1063/1.3692612
- Rogan, J., García, G., Valdivia, J. A., Orellana, W., Romero, A. H., Ramírez, R., et al. (2005). Small pd clusters: a comparison of phenomenological and ab initio approaches. *Phys. Rev. B* 72:115421. doi: 10.1103/PhysRevB.72.115421
- Rupp, M., Tkatchenko, A., Müller, K.-R., and von Lilienfeld, O. A. (2012). Fast and accurate modeling of molecular atomization energies with machine learning. *Phys. Rev. Lett.* 108:058301. doi: 10.1103/PhysRevLett.108.058301
- Sadeghi, A., Ghasemi, S. A., Schaefer, B., Mohr, S., Lill, M. A., and Goedecker, S. (2013). Metrics for measuring distances in configuration spaces. *J. Chem. Phys.* 139:184118. doi: 10.1063/1.4828704
- Saha, K., Agasti, S. S., Kim, C., Li, X., and Rotello, V. M. (2012). Gold nanoparticles in chemical and biological sensing. *Chem. Rev.* 112, 2739–2779. doi: 10.1021/cr2001178
- Schön, J., Putz, H., and Jansen, M. (1996). Studying the energy hypersurface of continuous systems—the threshold algorithm. *J. Phys.* 8:143. doi: 10.1088/0953-8984/8/2/004

- Shayeghi, A., Götz, D., Davis, J. B., Schäfer, R., and Johnston, R. L. (2015a). Pool-BCGA: a parallelised generation-free genetic algorithm for the ab initio global optimisation of nanoalloy clusters. *Phys. Chem. Chem. Phys.* 17, 2104–2112. doi: 10.1039/C4CP04323E
- Shayeghi, A., Götz, D., Johnston, R., and Schäfer, R. (2015b). Optical absorption spectra and structures of ag 6+ and ag 8+. *Eur. Phys. J. D* 69:152. doi: 10.1140/epjd/e2015-60188-2
- Shayeghi, A., Heard, C. J., Johnston, R. L., and Schäfer, R. (2014). Optical and electronic properties of mixed ag-au tetramer cations. *J. Chem. Phys.* 140:054312. doi: 10.1063/1.4863443
- Shi, L.-T., Wang, Z.-Q., Hu, C.-E., Cheng, Y., Zhu, J., and Ji, G.-F. (2019). Possible lower energy isomer of carbon clusters c (n = 11, 12) via particle swarm optimization algorithm: Ab initio investigation. *Chem. Phys. Lett.* 721, 74–85. doi: 10.1016/j.cplett.2019.02.028
- Shi, Y.-K., Li, Z. H., and Fan, K.-N. (2010). Validation of density functional methods for the calculation of small gold clusters. *J. Phys. Chem. A* 114, 10297–10308. doi: 10.1021/jp105428b
- Shinde, R., and Shukla, A. (2014). Large-scale first principles configuration interaction calculations of optical absorption in aluminum clusters. *Phys. Chem. Chem. Phys.* 16, 20714–20723. doi: 10.1039/C4CP02232G
- Solov'yov, I. A., Solov'yov, A. V., and Greiner, W. (2004). Fusion process of lennard-jones clusters: global minima and magic numbers formation. *Int. J. Mod. Phys. E* 13, 697–736. doi: 10.1142/S0218301304002454
- Song, C., Ge, Q., and Wang, L. (2005). Dft studies of pt/au bimetallic clusters and their interactions with the co molecule. *J. Phys. Chem. B* 109, 22341–22350. doi: 10.1021/jp0546709
- Stewart, J. (2016). *Mopac 16*. Colorado Springs, CO: Stewart Computational Chemistry.
- Turney, J. M., Simonett, A. C., Parrish, R. M., Hohenstein, E. G., Evangelista, F. A., Fermann, J. T., et al. (2012). Psi4: an open-source ab initio electronic structure program. *Wiley Interdiscip. Rev.* 2, 556–565. doi: 10.1002/wcms.93
- Wales, D. J., and Scheraga, H. A. (1999). Global optimization of clusters, crystals, and biomolecules. *Science* 285, 1368–1372. doi: 10.1126/science.285.5432.1368
- Weigend, F., and Ahlrichs, R. (2005). Balanced basis sets of split valence, triple zeta valence and quadruple zeta valence quality for h to rn: Design and assessment of accuracy. *Phys. Chem. Chem. Phys.* 7, 3297–3305. doi: 10.1039/b508541a
- Wen, J.-Q., Chen, G.-X., Zhang, J.-M., and Wu, H. (2018). The study of structures and properties of pdnhm(n = 1–10, m = 1,2) clusters by density functional theory. *J. Phys. Chem. Solids* 115, 84–91. doi: 10.1016/j.jpics.2017.12.011
- Xiao, C., Krüger, S., Belling, T., Mayer, M., and Rösch, N. (1999). Relativistic effects on geometry and electronic structure of small pdn species (n = 1, 2, 4). *Int. J. Quant. Chem.* 74, 405–416.
- Zacarias, A. G., Castro, M., Tour, J. M., and Seminario, J. M. (1999). Lowest energy states of small pd clusters using density functional theory and standard ab initio methods. a route to understanding metallic nanoprobles. *J. Phys. Chem. A* 103, 7692–7700. doi: 10.1021/jp9913160
- Zhang, J., and Dolg, M. (2015). Abcluster: the artificial bee colony algorithm for cluster global optimization. *Phys. Chem. Chem. Phys.* 17, 24173–24181. doi: 10.1039/C5CP04060D
- Zhao, Y., Chen, X., and Li, J. (2017). Tgmin: a global-minimum structure search program based on a constrained basin-hopping algorithm. *Nano Res.* 10, 3407–3420. doi: 10.1007/s12274-017-1553-z

**Conflict of Interest:** The authors declare that the research was conducted in the absence of any commercial or financial relationships that could be construed as a potential conflict of interest.

Copyright © 2019 Khatun, Majumdar and Anoop. This is an open-access article distributed under the terms of the Creative Commons Attribution License (CC BY). The use, distribution or reproduction in other forums is permitted, provided the original author(s) and the copyright owner(s) are credited and that the original publication in this journal is cited, in accordance with accepted academic practice. No use, distribution or reproduction is permitted which does not comply with these terms.